Molecular Therapy
Original Article

Bispecific BAFF-R/BCMA CAR T cells control growth of heterogeneous plasma cells in multiple myeloma

Agnese Fiori,[1] Karin Zimmermann,[1] Anna Li,[2] Jörg Westermann,[3] Ioannis Anagnostopoulos,[4] Lutz Menzel,[1] Mario Bunse,[2] Henry Erdlei,[1] Jeyan Jayarajan,[2] Florian Grünschläger,[5,6] Juan Pablo Ortiz-Aguirre,[1,3] Simon Haas,[7,8,9,10] Uwe-Jens Teßmann,[11] Jens Freitag,[11] Andreas Rosenwald,[4] Larry Kwak,[12] Xiuli Wang,[12] Zhenyuan Dong,[12] Soungchul Cha,[12] John Reiser,[13] Eigen Peralta,[13] Bahram Valamehr,[13] Jan Krönke,[9] Uta E. Höpken,[2] and Armin Rehm[1]

[1]Max-Delbrück-Center for Molecular Medicine, Department of Translational Tumorimmunology, 13125 Berlin, Germany; [2]Max-Delbrück-Center for Molecular Medicine, Department of Microenvironmental Regulation in Autoimmunity and Cancer, 13125 Berlin, Germany; [3]Charité-University Medicine Berlin, Department of Hematology, Oncology and Tumorimmunology, Campus Virchow Klinikum, 13353 Berlin, Germany; [4]University of Würzburg, Institute of Pathology, 97080 Würzburg, Germany; [5]Heidelberg Institute for Stem Cell Technology and Experimental Medicine (HI-STEM gGmbH), 69120 Heidelberg, Germany; [6]Division of Stem Cells and Cancer, German Cancer Research Center (DKFZ), 69120 Heidelberg, Germany; [7]Berlin Institute of Health (BIH), 10178 Berlin, Germany; [8]Max-Delbrück-Center for Molecular Medicine, BIMSB, Berlin, Germany; [9]Charité-University Medicine Berlin, Department of Hematology, Oncology and Tumorimmunology, Campus Benjamin Franklin, 12203 Berlin, Germany; [10]Precision Healthcare University Research Institute, Queen Mary University of London, London E1 1HH, UK; [11]Helios Klinik Berlin-Buch, Department of Trauma Surgery, 13125 Berlin, Germany; [12]Toni Stephenson Lymphoma Center, Hematologic Malignancies Research Institute, Beckman Research Institute of City of Hope, Duarte, CA 91010, USA; [13]Fate Therapeutics, San Diego, CA 92131, USA

Multiple myeloma treatment has experienced tremendous advances through chimeric antigen receptor (CAR) therapies directed to the B cell maturation antigen (BCMA), but remissions are usually transient. To mitigate the risk of BCMA immune escape, we aimed for a simultaneous targeting of BCMA together with the B cell-activating factor receptor (BAFF-R). Single-cell RNA sequencing discovered increased BAFF-R gene (*TNFRSF13C*) expression in relapsed and refractory multiple myeloma cases, and it emerged as prognostic marker for long-term complete responses. BAFF-R was expressed in plasma cells at earlier maturation stages compared with BCMA-positive plasma cell phenotypes. Bispecific BAFF-R/BCMA CARs endowed T cells with cytolytic efficacy against multiple myeloma cell lines and primary multiple myeloma cells. *In vivo*, the dual CAR compensated for BCMA downregulation when BAFF-R was expressed, preventing the evolution of antigen escape mutants that drive resistance to CAR T cell therapy. Our study proposes BAFF-R as a complementary target antigen suitable to eliminate malignant plasma cells with less advanced differentiation, lack of BCMA, and occurrence in dismal prognosis patients.

INTRODUCTION

Multiple myeloma (MM) is a plasma cell (PC) malignancy with a high degree of molecular and immunophenotypic heterogeneity. Although treatment options over the past two decades have improved and led to prolonged overall survival,[1–3] therapy-imposed selective pressure in combination with the natural tumor evolution have impeded a definite cure of patients. B cell maturation antigen (BCMA) chimeric antigen receptor (CAR) T cell therapy has emerged as a revolutionary treatment option for patients with relapsed and refractory (R/R) disease. Two FDA-approved BCMA-specific CAR T cell products showed high response rates; however, this therapy is not considered curative.[4–7] BCMA-negative MM cells constitute a reservoir of treatment-refractory malignancy that can progress to clinical relapse.[8–10] Thus, responses of MM to BCMA CAR T cells are frequently not durable. Although antigen loss is only one of several mechanisms that account for MM relapse, immune escape has prompted multiple approaches to overcoming BCMA-negative relapses through simultaneous targeting of an additional PC-associated antigen. Identification of G protein-coupled receptor class C group 5 member D (GPRC5D) expression on $CD138^+$ primary MM cells informed the generation of CAR T cells incorporating a GPRC5D-targeted scFv. In a phase I study, GPRC5D CAR T cells elicited a 71% response rate in the entire cohort and across all dose levels, which is lower than for the pivotal BCMA CAR T cell trials.[11] A bicistronic CAR targeting BCMA and GPR5CD suggested a superior preclinical efficacy for eliminating BCMA-negative MM.[12] In a phase I clinical trial, MM patients were treated with a combination of monotargeted BCMA CAR and CD19 CAR

Received 31 January 2025; accepted 1 December 2025;
https://doi.org/10.1016/j.ymthe.2025.12.005.

Correspondence: Armin Rehm, MD, Department of Translational Tumorimmunology, Max-Delbrück-Center for Molecular Medicine, Berlin, Germany.
E-mail: arehm@mdc-berlin.de

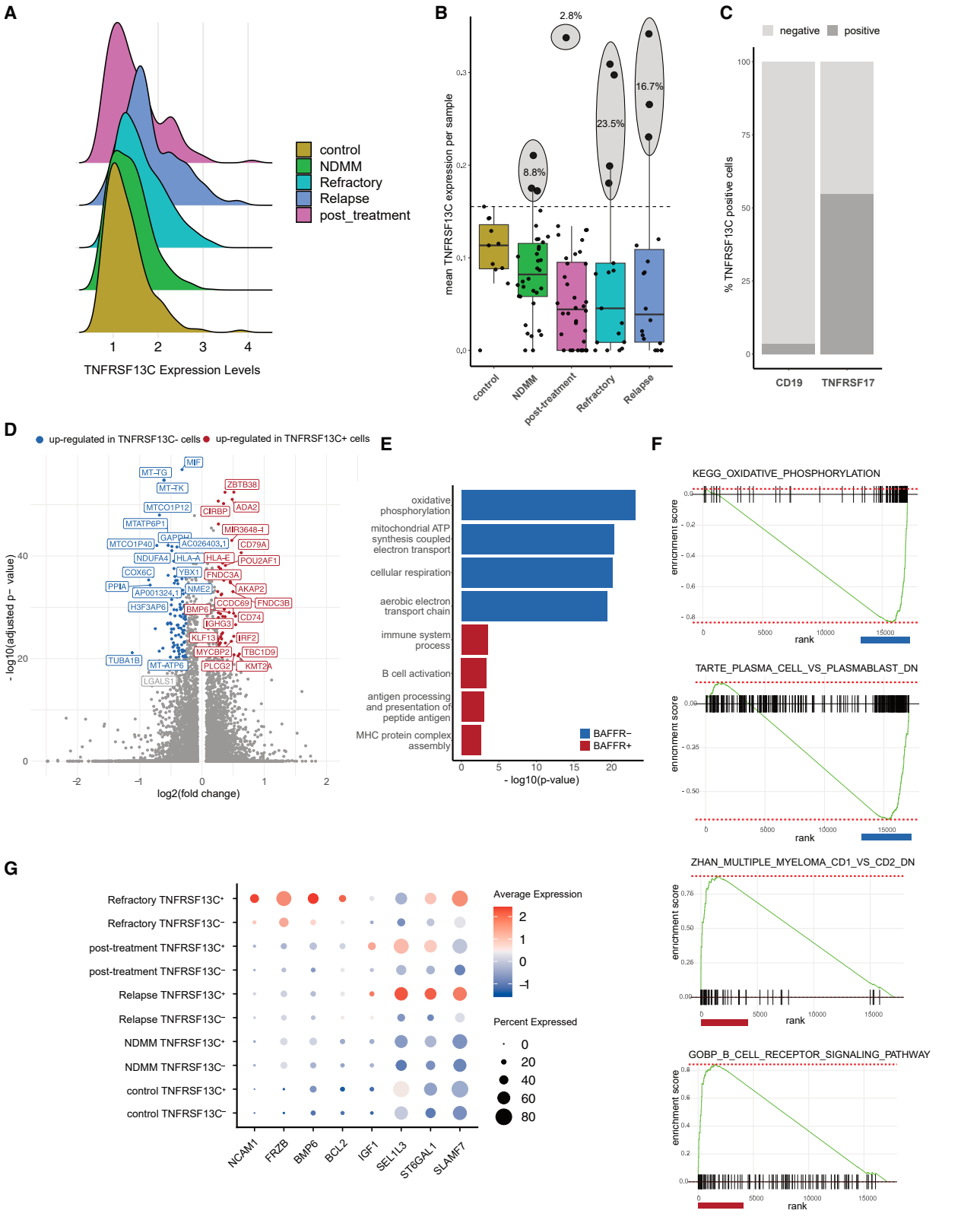

(legend on next page)

T cells. An early efficacy evaluation revealed similar response rates for the combined CAR and the single BCMA CAR T cell approach.[13] An important consideration in MM treatment resistance is the dependency on the bone marrow (BM) microenvironment. Interactions between cellular constituents and transformed PCs are mediated by the ligands for the B cell growth and differentiation receptors BCMA, TACI, and B cell-activating factor receptor (BAFF-R).[14,15] In the myeloid compartment, the ligand BAFF was upregulated and correlated with shorter progression-free survival (PFS).[16] In normal B cell development, these receptors have distinct, B cell differentiation-dependent expression. BCMA is predominantly expressed in mature PCs, while TACI also occurs in $CD27^+$ memory B cells, BM PCs, $CD27^-$ non-germinal center (GC) B cells, in a portion of naive B cells, but also in monocytes, macrophages, and DCs.[17] To target the PC-associated growth factor receptors concomitantly, a CAR construct incorporated their natural ligand APRIL as the binding domain for antigen-specific recognition.[18,19] However, a clinical study failed to show efficacy (NCT 03287804). A preclinical study demonstrated the capacity of a BAFF-ligand-based CAR to target MM cells, but a broad benign tissue targeting of cells expressing either TACI, BCMA, or BAFF-R raises concern regarding clinical translatability. In addition, the BAFF binder seems to endow CAR T cells with only modest avidity and antigen sensitivity, compared with a BCMA CAR.[20,21] Problematic with ligand-based CAR binders is their inherent stimulatory activity on tumor cells, without effectuating rapid cytotoxicity.[22] A broad cell lineage targeting of MM was suggested by the design of bispecific anti-BCMA/anti-TACI CAR constructs that exhibited promising preclinical efficacy.[22] BAFF-R expression starts on transitional stage B cells and lasts during their maturation into follicular and marginal zone B lymphocytes, but is also expressed in memory B cells. Long-lived PCs are usually devoid of the receptor.[23–25] Here, we focused on antigens with broad expression on mature B cells and PCs. Notably, a search in cell lines for such antigens can be misleading because they are usually derived from PC leukemia or extramedullary myeloma, with different biological behavior compared with primary BM-derived MM cells. We generated a dual BAFF-R/BCMA CAR that recognizes two MM-associated target antigens reflecting heterogeneous maturation stages. Whereas BCMA is expressed with high prevalence on mature malignant PCs, the occurrence of BAFF-R on malignant PCs with more B cell-like phenotypes allows for a complementary targeting approach. We show that BAFF-R is increasingly expressed in R/R disease stages. Patients with high BAFF-R (*TNFRSF13C*) gene expression at initial diagnosis (ID) are more likely to fail in achieving complete remissions (CRs). Thus, BAFF-R is a prediction marker for an adverse clinical outcome. Simultaneous targeting of BCMA and BAFF-R may fill the gap in the capacity of monotargeted BCMA CARs to eradicate residual BCMA-negative tumor cells that preexist or that evolve upon selective pressure.

RESULTS

TNFRSF13C is upregulated in a subset of progressive MM cases

Previous data showed surface expression of BAFF-R in a small cohort of primary MM BM specimens.[25] To quantify intensity and distribution of BAFF-R gene (*TNFRSF13C*) expression, we integrated single-cell RNA sequencing data (scRNA-seq) from two published studies.[26,27] In total, 116 samples enriched for $CD38^+$/$CD138^+$ PC were included. MM samples displayed a great inter-patient heterogeneity in mRNA expression in the Uniform Manifold Approximation and Projection (UMAP) (Figure S1A), but samples originating from the same patient co-localized. Expression of genes associated with hematological malignancies such as *NCMA1* (CD56) and *KIT* were found outside the area associated with benign samples (Figure S1B). Compared with *CD19*, *TNFRSF13C*-expressing cells were more prevalent. Elevated CD24 on malignant PCs is correlated with extended PFS.[28] In our analysis, $CD24^+$ PCs occurred at a low frequency. *MS4A1* (CD20), indicative of mature B cells and of t(11;14) translocation in MM with small mature PC morphology,[29] was found in cells from several samples (Figure S1B). Genes characterizing a molecular signature of MM[30] revealed some group-specific patterns (Figure S1C). *TNFRSF13C* mRNA expression was undetectable in MM cell lines (Figure S1D).

TNFRSF13C average gene expression was considerably higher for the relapsed, post-treatment and refractory cohorts (Figure 1A). Averaging *TNFRSF13C* gene expression by patient (Figure 1B) showed that, in 17% of the relapsed cases and in 24% of the patients being refractory to chemo- or antibody therapy, this marker was about 2-fold increased compared with average expression levels of newly diagnosed MM (NDMM). Only about half of the $TNFRSF13C^+$ PCs co-expressed *TNFRSF17* (BCMA) (Figure 1C).

To elucidate the relevance of a dual targeting approach for this group, we deeper analyzed (Figure S2A) patients with high average BAFF-R (*TNFRSF13C*) expression. While control and NDMM patients showed a positive correlation of BAFF-R and BCMA, in R/R

Figure 1. *TNFRSF13C* expression correlates with disease severity and cancer driver gene expression

(A) Gene expression of *TNFRSF13C* (BAFF-R) by disease group increases with disease stage and treatment resistance. (B) Average *TNFRSF13C* gene expression by patient diverges dependent on disease stage and select patient subsets. Each data point is representative of one patient. Dotted line, arbitrary gene expression level of healthy control PCs. (C) Stacked bar graphs show that MM cells displaying *TNFRSF13C* do not co-express *TNFRSF17* (BCMA) in 45% of the cases. (D) Volcano plot of the top differentially expressed genes between *TNFRSF13C*-positive and -negative malignant PCs. Genes significantly upregulated ($p < 0.05$) in $TNFRSF13C^-$ cells are depicted in blue, and those upregulated in $TNFRSF13C^+$ PCs are in red. (E) Gene Ontology (GO) pathway analysis of the top DEGs in $TNFRSF13C^-$ (blue bar) versus $TNFRSF13C^+$ cells (red bar). Genes upregulated in $TNFRSF13C^+$ MM cells are enriched for B cell-mediated immune responses. (F) GSEA of DEG reveals an enrichment of a plasmablastic signature (in blue box), whereas GSEA in the red box contains genes discriminative for the MM signatures CD1 and CD2. (G) Cancer driver genes from an MM signature are disease stage dependently upregulated in $TNFRSF13C^+$ PCs. Dot plot representing the size-coded percentage of $BAFF\text{-}R^-$ and $BAFF\text{-}R^+$ cells expressing selected MM signature genes. Average gene expressions are depicted according to the color scale.

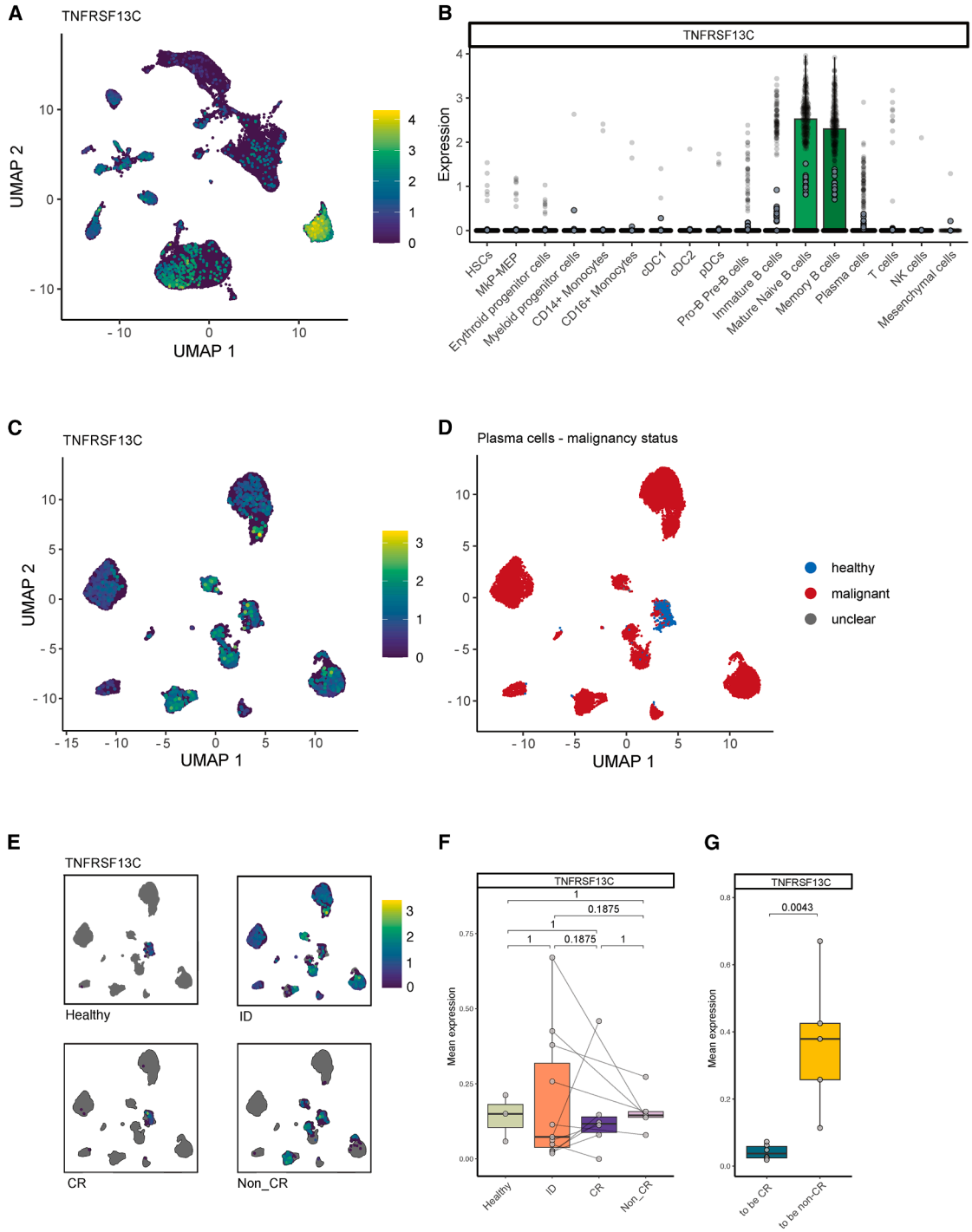

Figure 2. A longitudinal study of MM patients elucidates the prognostic potential of *TNFRSF13C*

(A) Global UMAP display of scRNA-seq data of BM from healthy donors (n = 3), paired samples from 11 MM long-term survivor patients at ID and long-term survival (LTS), including color-coded *TNFRSF13c* expression. *TNFRSF13c*-positive cells are colored in green. (B) *TNFRSF13C* expression by benign cell type, indicating restriction to memory and mature naive B cells. (C) UMAP of the PC clusters from all patients with color-coded *TNFRSF13C* expression. (D) Benign PCs of different patients cluster together (in gray), while malignant PCs show an inter-patient heterogeneity (in red). (E) UMAP of PC compartment split by all clinical groups; healthy controls, initial diagnosis (ID), complete remission (CR), and non-CR. *TNFRSF13C*$^+$ PC abundance and distribution is color-coded. (F) Boxplot showing paired mean *TNFRSF13C* expression

(legend continued on next page)

patients BCMA negatively correlated with increasing BAFF-R expression. We hypothesize that BAFF-R positive MM cells might fuel relapse or refractory behavior.

Next, we examined differentially expressed genes (DEGs) between *TNFRSF13C*$^{-}$ and *TNFRSF13C*$^{+}$ PCs (Figure 1D). The Volcano plot showed that the *TNFRSF13C*$^{-}$ group of cells (blue) overexpressed mostly mitochondrial genes (i.e., *COX6C*, *MTCO1P12*), whereas *TNFRSF13C*$^{+}$ cells (red) exhibited higher expression of B cell signaling-associated genes and immunoregulators. *CD74* initiates cell proliferation and survival pathways,[31] and *CD79A* is associated with the BCR complex and a top-ranking gene upregulated in PCs.[32] CCDC69 mediates localization of AURKB to the mitotic spindle midzone and, thus, contributes to MM cell-cycle progression.[33] *CIRBP* has an oncogenic function in various cancer types by inducing *HIF-1a*,[34] mRNA stabilization, and enhancement of translation. Upregulation of *HLA-E* points to an immune checkpoint function through interaction with CD94/NKG2A on NK cells.[35]

Gene Ontology analysis confirmed enriched signatures related to cellular energy supply in *TNFRSF13C*$^{-}$ cells, whereas *TNFRSF13C*$^{+}$ cells expressed gene sets associated with a B cell-like phenotype and immune response (Figure 1E). Gene set enrichment analysis (GSEA) indicated a significant enrichment of CD2 subtype-specific genes (compared with CD1) in genes more prominently expressed in *TNFRSF13C*$^{+}$ cells.[30] In addition, a plasmablastic signature[36] was enriched in genes highly expressed in *TNFRSF13C*$^{-}$ cells (Figure 1F). For *TNFRSF13C*$^{+}$ MM cells, we found in the refractory cohort upregulation of *NCAM1*, *FRZB*, *BMP6*, and *BCL2* (Figure 1G). NCAM1 (CD56) induces the activation of the RSK2/CREB1 signaling pathway, with increased expression of the anti-apoptotic genes *BCL2* and *MCL1*.[37] FRZB stimulates the Wnt-signaling pathway, thereby mediating proliferation, migration, and drug resistance.[38] In the post-treatment group, *TNFRSF13C*$^{+}$ PCs showed elevated levels of the growth factor receptor *IGF1* (Figure 1G).[39] Collectively, gain of differential gene functions may support the treatment resistance of *TNFRSF13C*$^{+}$ MM cells.

BAFF-R expression correlates with an adverse prognosis in a longitudinal MM patient study

We asked whether a link between *TNFRSF13C* expression levels at ID and at more advanced disease stages existed. We analyzed a scRNA-seq dataset from BM aspirates from healthy donors and MM patients (Figure 2A).[40] The study included 24 MM paired samples from patients at ID and upon long-term survival (LTS) between 7 and 17 years after first-line therapy.[40] For 11 of them, paired scRNA-seq data could be analyzed. Mature naive B cells and memory B cells exhibited the highest *TNFRSF13C* mRNA content (Figure 2B). Next, we zoomed in on the PC subpopulation (Figure 2C) and integrated expression data for healthy and MM PCs, confirming a considerable prevalence of *TNFRSF13C*$^{+}$ cells among malignant PCs (Figures 2C and 2D). CR status after therapy was associated with a strong reduction of malignant PCs, including reduction of the *TNFRSF13C*$^{+}$ PC cluster. In contrast, non-CR patients, who are prone to relapse, still maintained or had developed abundant PC subsets with *TNFRSF13C* expression (Figure 2E).

When comparing matched-pairs of MM patients at ID and LTS, split by CR and non-CR in this longitudinal study cohort, we found that *TNFRSF13C* expression levels between these three groups showed no significant changes in the pairwise comparisons (Figure 2F). However, when comparing patients that acquired durable CR and those with biochemical progression (non-CR), all CR patients had overall lower *TNFRSF13C* expression at ID (Figure 2G). In conclusion, *TNFRSF13C* expression status at ID emerged as a prediction marker for LTS.

Primary MM cells express BAFF-R protein in several cases and in a subset of cells

Previous studies have demonstrated BAFF-R expression in a variety of lymphoproliferative malignant diseases.[41,42] In addition, in a surfaceome study of MM, BAFF-R occurred in the top 1% of targets when a combined evaluation of gene expression and protein data was applied (Figure S2B).[43] We performed immunohistochemistry (IHC) on BM biopsies and extramedullary manifestations from 58 MM cases. Among the 20 NDMM patients, BAFF-R expression in CD138^{+} PCs was detected in 11 cases (Table S1). The number of positive cells per case was highly variable, ranging from 5% to 90% of the neoplastic cells (Figure 3A). In the post-treatment group comprising relapsed disease ($n = 30$), BAFF-R was expressed in 13 cases, yet with a wide frequency range of labeled cells (10%–100%). In a matched-pairs longitudinal observation of 10 patients having BM biopsies at ID and at two follow-up time points, four cases exhibited constantly absent BAFF-R expression. Four cases showed varying numbers of labeled PCs during the disease course (e.g., case no. 1: 10%–30%–40%). None of the eight cases with extramedullary manifestations exhibited BAFF-R expression (Table S1). Overall, BAFF-R was found in 55% of NDMM and in 43.44% of post-treatment patients (Figure 3B). Differences from NDMM frequencies in scRNA-seq (Figure 1B) may result from the methodological selection of CD138^{+}CD38^{+} PCs. In addition, patient inclusion criteria in these two cohorts were not stratified for complementarity.

In flow cytometry analysis (FACS) all cell lines expressed BCMA, but not BAFF-R (Figure 3C). Primary MM samples were routinely diagnosed in the clinic by the combinatorial expression of

summarized for each patient and split between the clinical states, healthy donors, patients at ID, and LTS split into CR and non-CR patients. Changes between clinical states are not significant. Non-paired Wilcoxon test for healthy versus others; and comparison CR versus non-CR; paired Wilcoxon test for ID with CR and non-CR. *p* values adjusted for multiple comparison. Data points indicate individual patients. (G) Mean *TNFRSF13c* expression summarized for each patient at ID and split for their clinical outcome at LTS into CR and non-CR. Significance tested using unpaired two-sample Wilcoxon test.

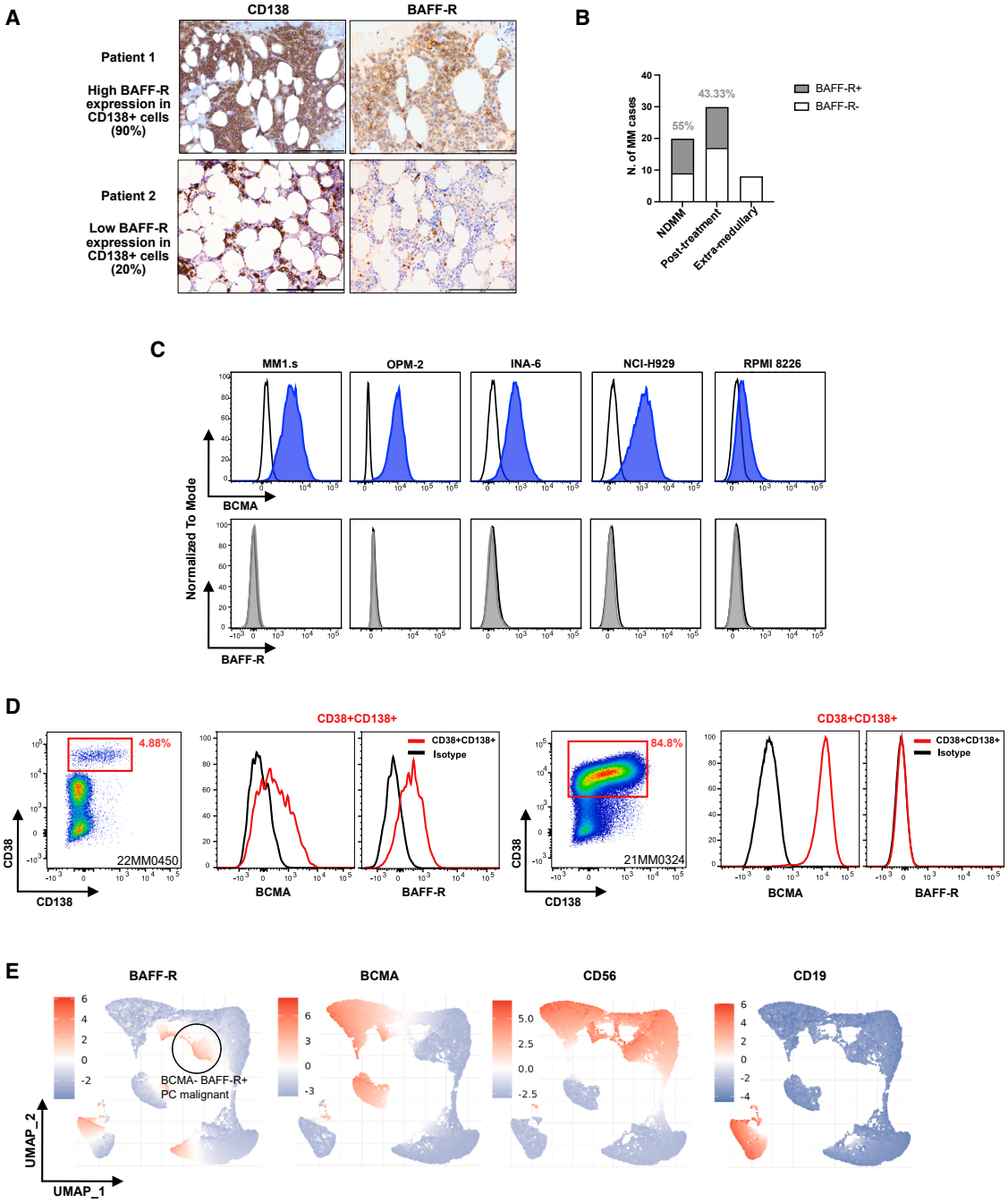

Figure 3. BAFF-R is abundantly expressed in malignant primary MM BM specimens

(A) Representative immunohistochemical detection of BAFF-R on malignant PCs. Primary BM biopsies with MM diagnosis were stained to evaluate BAFF-R expression, and identification of neoplastic PCs by CD138+ staining. Representative images. Scale bars, 100 μm (patient 1) and 200 μm (patient 2). (B) Stacked bar graphs for quantitation of BAFF-R$^+$ PC frequencies. *n* = 20 cases with newly diagnosed multiple myeloma (NDMM) biopsies, *n* = 30 post-treatment cases and *n* = 8 cases in final disease stage with extramedullary MM manifestations. (C) Flow cytometric analysis of surface expression of BCMA (blue) and BAFF-R (gray) on MM cell lines. Isotype control, black open histogram. (D) Representative gating strategy for the detection of malignant PCs within two individual BM-derived MM samples (nos. 22MM0450 and 21MM0324). Malignant PCs are identified as CD38$^+$CD138$^+$. BCMA and BAFF-R expression in this gated population was evaluated. CD38$^+$CD138$^+$, red open histogram; isotype control, black open histogram. (E) UMAP displays BAFF-R, BCMA, CD56, and CD19 surface expression within CD38$^+$CD138$^+$ PCs from all evaluated specimen (MM, *n* = 33; healthy control, *n* = 5).

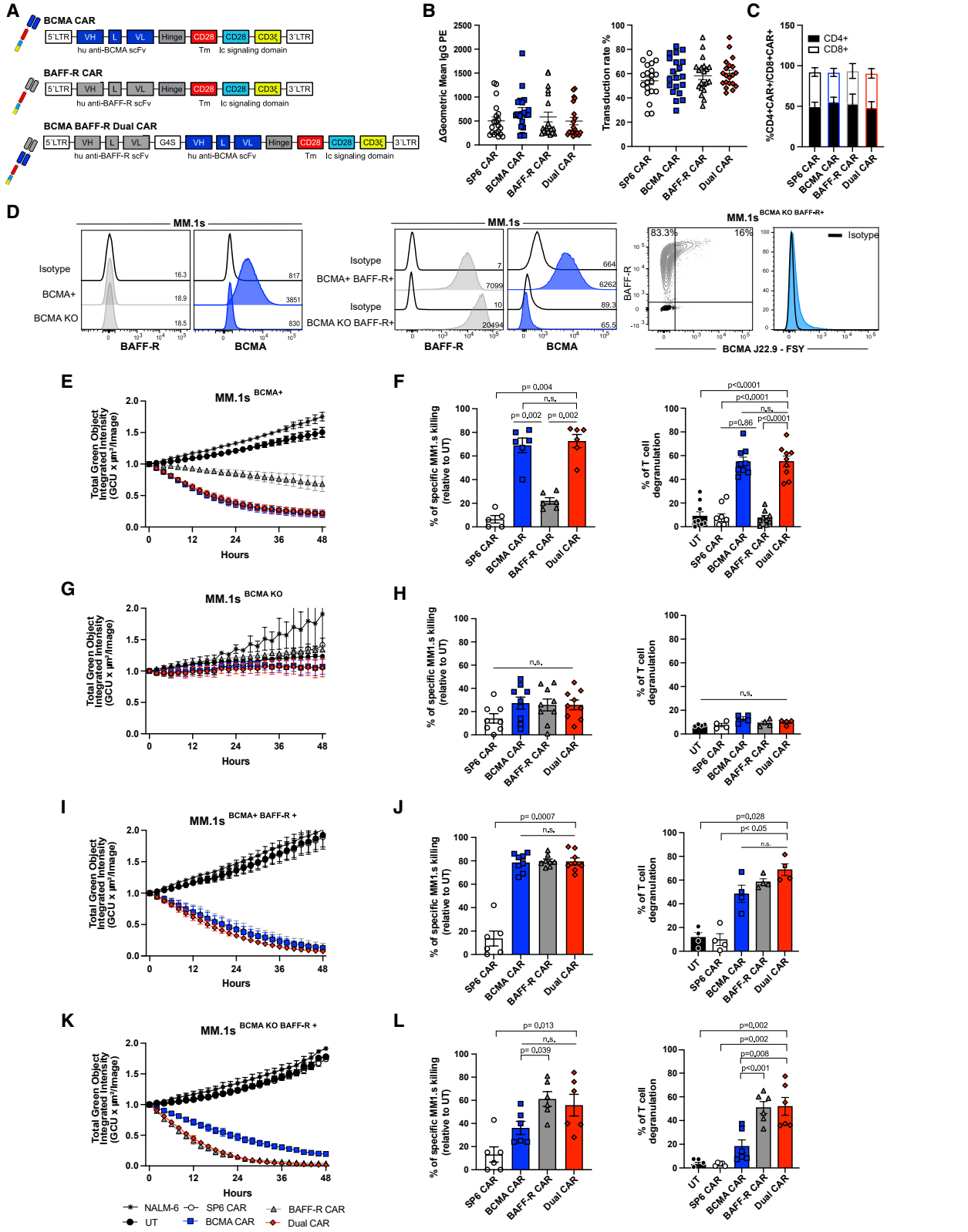

(legend on next page)

$CD45^{dim}CD138^{+}CD38^{+high}CD19^{-}Ig\kappa^{+}$ or $Ig\lambda^{+}$. To further resolve MM immunophenotypes, we applied an informative antibody panel (CD3/CD138/CD38/CD56/BCMA/CD19/BAFF-R; Figures S3A and S3B). Malignant PCs were defined as $CD3^{-}CD38^{+(high)}CD138^{+}$, and their frequencies were highly variable ranging from 1% to 85% (Figures 3D and S3C). In one-third of the cases, BAFF-R expression was found to a different extent and always co-expressed with BCMA. Notably, the intensity of BAFF-R staining in malignant PCs was usually dimmer than that in $CD19^{+}$ B cells (Figure S3A). Collectively, frequent occurrence of BAFF-R in malignant PCs fulfills the expectation on a targetable tumor-associated antigen in MM.

UMAP of malignant PCs from all analyzed cases visualized a predominant cluster of $CD19^{-}$ PCs which mainly co-expressed CD56, a frequent marker for transformed PCs[37] (Figure 3E). Among this subset ($CD138^{+}CD38^{+(high)}CD19^{-}CD56^{+}$), half of the cells co-expressed BCMA (17/33 cases), and a further subset also exhibited BAFF-R (8/33). In total, 11/33 primary MM cases exhibited BAFF-R surface expression. UMAP visualized a cluster of malignant PCs being positive for BAFF-R but not for BCMA. In healthy BM, $CD138^{+}CD38^{+(high)}$ PCs occurred in very low frequencies co-expressing BCMA and BAFF-R. In contrast to malignant PCs, they were all $CD19^{+}$ (Figure S3B). Together, variable expression of BAFF-R and BCMA in malignant PC subsets and the identification of clusters solely positive for one or the other antigen contributes to disease heterogeneity in MM.

Dual CAR T cells are as efficient as BCMA CAR T cells against BCMA-positive MM cell lines *in vitro*

Gene expression data in conjunction with the validation of BAFF-R protein expression in primary MM cases prompted us to target BAFF-R and BCMA simultaneously. The BCMA CAR construct was previously reported.[21] Key features are a humanized anti-BCMA scFv with high affinity (K_D = 2.2 nM) and the capacity to recognize cell lines with less than 100 molecules of BCMA.[44] The anti-BAFF-R CAR uses a humanized scFv (K_D < 4 nM; data from patent WO2017214170A2) and has been reported as a favorable alternative to CD19 CAR T cells, demonstrating clinical safety and efficacy in currently recruiting clinical trials for B cell malignancies (NCT04690595; NCT05370430).[42,45]

For dual targeting, we explored dual-scFv (tandem) CAR (referred to as dual CAR, Figure 4A) and bicistronic CAR configurations (Figure S4A). After retroviral transduction in human T cells, the monotargeted CARs, an SP6 control CAR, and the dual CAR construct had comparable transduction efficiencies, surface densities, and CD4/CD8 ratios (Figures 4B and 4C). The bicistronic constructs had substantially lower transduction efficiencies (mean 20%) (Figure S4B). Although bicistronic CAR T cells were efficient in targeting $BCMA^{+}$ MM cell lines (MM1.s, RPMI-8226) and NALM-6 ($BAFF\text{-}R^{+}$) (Figures S4C–S4G), we here favored the tandem CAR design with superior transduction rates and higher retroviral titers. Both properties are critical for patient-derived leukapheresis material that is impaired after multiple exposures to myelosuppressive chemotherapies. Moreover, DNA recombination events due to large sequence overlaps in bicistronic CAR designs can lead to intramolecular template switching and less-efficient dual CAR expression.[46]

For the dual CAR (Figure 4A), we first evaluated the specificity of BCMA targeting comparing monotargeted BCMA CAR and the dual CAR T cells in coculture with the $MM.1s^{BCMA+}$ cell line ($BAFF\text{-}R^{-}$). To monitor specificity, we generated $MM.1s^{BCMA\ KO}$ cells. BCMA expression on $MM.1s^{BCMA+}$ and on $MM.1s^{BCMA\ KO}$ cells was confirmed by FACS using the mouse antibody 19F2 (Figure 4D, left, middle panel). Target cells were further validated by staining with the recombinant antibody J22.9-FSY, which is incorporated as scFv into our BCMA CAR (Figure 4D, right panel).[21,44] The $MM.1s^{BCMA+}$ cell population was progressively eliminated when cocultured with

Figure 4. Dual targeted CAR T cells in a tandem configuration specifically lyse BCMA-expressing MM.1s target cells

(A) Schematics of CAR constructs. VH, variable heavy chain; VL, variable light chain; L, Whitlow linker; Tm, transmembrane region; Ic, intracellular signaling domain; LTR, long terminal repeat; hinge, human IgG1 constant region; G4S, poly-glycine-serine linker. (B) CAR surface expression on transduced T cells. Expression levels are given as gMFI values, transduction rates in percent of T cells. Data are mean ± SEM, *n* = 20 independent T cell donors. (C) $CD4^{+}/CD8^{+}$ ratios (in percent) of transduced CAR T cells; mean ± SEM, *n* = 4 independent T cell donors per construct. (D) Left and middle panel: BAFF-R (gray) and BCMA (blue) antigen expression on $MM.1s^{BCMA+}$, $MM.1s^{BCMA\ KO}$, $MM.1s^{BCMA+\ BAFF\text{-}R+}$, and $MM.1s^{BCMA\ KO\ BAFF\text{-}R+}$ cells. Anti-BCMA antibody 19F2 was used; gMFI values are reported. Right panel: BCMA expression on $MM.1s^{BCMA\ KO\ BAFF\text{-}R+}$ (light blue) cells evaluated with anti-BCMA J22.9-FSY antibody. Isotype controls, black open histogram. In the contour plot, numbers in the gates are the percentages of $BCMA^{+}$ and $BCMA^{-}$ cells. (E) IncuCyte assay of CAR T cells in coculture with GFP^{+} $MM1.s^{BCMA+}$. Killing kinetic is reported as progressive decrease of total green object integrated intensity. Mean ± SEM. Untransduced (UT), *n* = 18; SP6 CAR, *n* = 20; BCMA CAR, *n* = 18; BAFF-R CAR, *n* = 16; dual CAR of *n* = 20 T cell donors; *n* = 11 independent assays. (F) Left panel: flow cytometry-based cytotoxicity assay of CAR T cells and $MM.1s^{BCMA+}$ in a 1:1 coculture. $MM.1s^{BCMA+}$ cell killing is reported as a percentage, calculated relative to coculture with UT T cells. Right: percentage of CAR T cell degranulation after 4 h of coculture with $MM.1s^{BCMA+}$ cells. (G) IncuCyte assay of CAR T cells in coculture with GFP^{+} $MM1.s^{BCMA\ KO}$. Mean ± SEM. UT, *n* = 3; SP6 CAR, *n* = 5; BCMA CAR, *n* = 5; BAFF-R CAR, *n* = 3; dual CAR of *n* = 5 T cell donors; *n* = 2 independent experiments. (H) Left: FACS assay of CAR T cells and $MM.1s^{BCMA\ KO}$. Killing is reported as a percentage, calculated relative to coculture with UT. Mean ± SEM. Right: CAR T cell degranulation in coculture with $MM.1s^{BCMA\ KO}$. (I) IncuCyte assay of CAR T cells in coculture with GFP^{+} $MM.1s^{BCMA+\ BAFF\text{-}R+}$. Data are mean ± SEM. U, *n* = 5; SP6 CAR, *n* = 5; BCMA CAR, *n* = 4; BAFF-R CAR, *n* = 4; dual CAR of *n* = 5 T cell donors; *n* = 6 independent experiments performed. (J) Left panel: FACS cytotoxicity assay of CAR T cells and $MM.1s^{BCMA+\ BAFF\text{-}R+}$. $MM.1s^{BCMA+\ BAFF\text{-}R+}$ cell killing is reported as a percentage, calculated relative to UT. Right: CAR T cell degranulation, coculture with $MM.1s^{BCMA+\ BAFF\text{-}R+}$. (K) Killing kinetic of CAR T cells in coculture with GFP^{+} $MM.1s^{BCMA\ KO\ BAFF\text{-}R+}$ target cells. Data are mean ± SEM. UT, *n* = 6; SP6 CAR, *n* = 8; BCMA CAR, *n* = 8; BAFF-R CAR, *n* = 6; dual CAR of *n* = 8 T cell donors; *n* = 7 independent experiments performed. (L) Left panel: cytotoxicity assay of CAR T cells and $MM.1s^{BCMA\ KO\ BAFF\text{-}R+}$. Right: percentage of CAR T cell degranulation in coculture with $MM.1s^{BCMA\ KO\ BAFF\text{-}R+}$. In (F, H, J, and L) statistics calculated by Mann-Whitney test, data points represent single CAR T cell donors. Data are mean ± SEM; n.s., not significant.

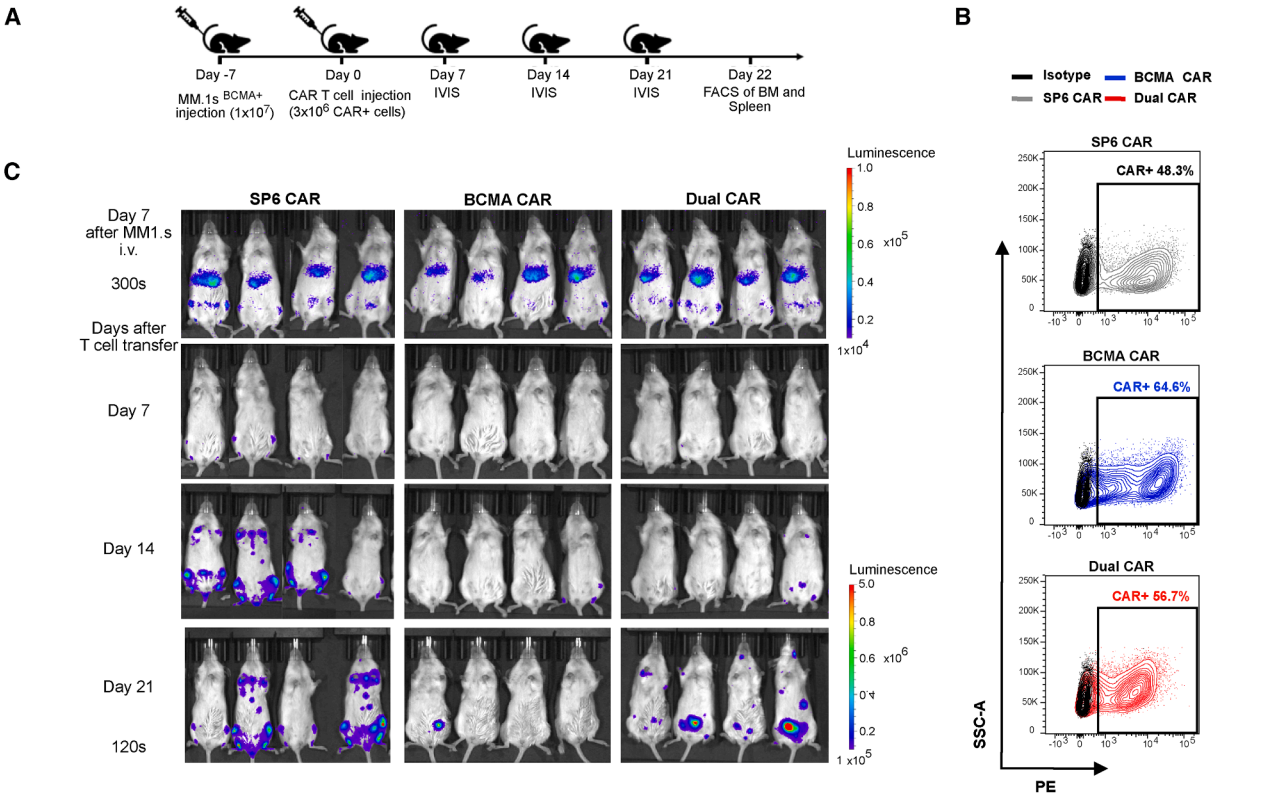

(legend on next page)

BCMA CAR and dual CAR T cells (Figure 4E). In a FACS-based cytotoxicity assay, BCMA CAR, and dual CAR T cells induced comparable killing (Figure 4F, left panel). The cytotoxic activity of the BCMA and dual CAR T cells was further confirmed by LAMP-1 degranulation assay (Figure 4F, right). MM.1s$^{BCMA\ KO}$ cells were spared from single and dual CAR-mediated tumor cell elimination (Figure 4G). In the FACS-based killing assay, reactivity against MM.1s$^{BCMA\ KO}$ cells was in the low background range of the SP6 control (Figure 4H, left panel). Results from a LAMP-1 assay were consistent with absence of BCMA (Figure 4H, right panel). Notably, the BAFF-R CAR T cells exhibited some background cytolytic activity in IncuCyte and FACS-based killing assays against MM.1s wild-type cells. The level of activity was significantly lower than for the BCMA CAR and the dual CAR, and did not occur in a LAMP-1 degranulation assay (Figure 4F). Similar results were obtained in cytotoxicity assays against the OPM-2 MM cell line (Figures S5B and S5C), indicating a modestly higher cytolytic activity of the BAFF-R CAR compared with the SP6 CAR. Potentially, tonic signaling in BAFF-R CAR T cells could contribute to the observed low reactivity against antigen-negative target cells.[47,48] When Jurkat cells carrying a stably integrated NF-κB eGFP fusion protein were transduced with our retroviral constructs, a 2- to 3-fold upregulation of eGFP in BAFF-R CAR transduced cells compared with the SP6 control CAR was obtained (Figure S6A). In accordance, gMFI values for HLA-DR expression on primary CD4$^+$ CAR T cells were much higher in BAFF-R CAR transduced T cells than in the SP6 CAR control group (Figure S6B). In summary, the BAFF-R CAR construct endows T cells with tonic signaling.

To generate MM.1s$^{BCMA\ KO\ BAFF\text{-}R+}$ cells, CRISPR-Cas9 technology was used to delete BCMA followed by multiple cell sorts with the anti-BCMA 19F2 antibody. Next, BCMA KO and MM.1s^{BCMA+} cells were transduced with BAFF-R. MM.1s$^{BCMA+\ BAFF\text{-}R+}$ and MM.1s$^{BCMA\ KO\ BAFF\text{-}R+}$ were cocultured with CAR T cells. The presence of both antigens on target cells induced MM.1s$^{BCMA+BAFF\text{-}R+}$ killing and T cell degranulation, comparable for both monotargeted CARs and the dual CAR (Figures 4I and 4J). IFN-γ release was higher in BAFF-R CAR T cells than in dual CAR T cells (Figure S5A, right panel).

Despite repetitive enrichment steps, staining on MM.1s$^{BCMA\ KO\ BAFF\text{-}R+}$ cells with the high-affinity BCMA J22.9-FSY antibody revealed a residual positivity for BCMA of around 15%–20% of the cells (Figure 4D, right panel). Accordingly, residual low BCMA expression in MM.1s$^{BCMA\ KO\ BAFF\text{-}R+}$ cells was detectable in an IncuCyte assay. The killing kinetics of the BCMA CAR was substantially delayed compared with the dual CAR T cells (Figure 4K). Similarly, in a FACS-based killing assay, the dual CAR and the BAFF-R CAR T cells had improved cytotoxic efficacy (Figure 4L). Degranulation and IFN-γ secretion were substantially higher in dual CAR than in BCMA CAR T cells, reflecting their superior activation in the presence of BAFF-R and low amounts of BCMA (Figures 4L and S5A).

Cytolytic efficacy against B-NHL cell lines DOHH-2 and JeKo-1 (BAFF-R$^+$BCMA^{low}) was comparable for the dual CAR and both monotargeted CAR T cell products (Figures S7A and S7B).

Dual CAR T cells limit disease progression *in vivo*

To assess the cytotoxic capacity of dual CAR T cells in a xenograft mouse model, we injected intravenously (i.v.) luciferized MM.1s^{BCMA+} cells which grow preferentially as orthotopic tumors in BM.[21] One week after injection, tumor growth was confirmed by bioluminescence imaging (BLI), followed by a single dose CAR T cell administration (2.5–3 × 10^6 CAR$^+$ cells, Figures 5A–5C). CAR T cells with similar transduction rates (50%–65%) were used (Figure 5B). In weekly imaging intervals, the SP6 control group exhibited a constant MM progression localized to the pelvic region and legs (Figure 5C). Animals treated with BCMA CAR T cells as well as those treated with the dual CAR T cells exhibited a comparable anti-tumor potency (Figure 5C) (average radiance value BCMA CAR: 3.1 × 10^7; dual CAR: 2 × 10^7; SP6: 1.1 × 10^8). Tumor load in BM (Figure 5D) and in spleen (Figure S8A, left panel) revealed a similar depletion in the BCMA CAR- and dual CAR T cell-treated cohorts. Among the groups, comparable amounts of CD3$^+$ and CAR T cells were found in BM and spleen (Figures 5E and S8A).

CAR T cells recovered from both compartments showed no major differences in frequencies and in expression of the exhaustion markers PD-1, LAG-3, or TIM-3 (BM, Figures 5F, spleen, and S8B). Differences in the CD4/CD8 T cell ratios in mice treated with SP6, BCMA, or dual CAR T cells were not obvious (BM CD4:CD8 mean values; SP6 CAR: 58:42%; BCMA CAR: 59:41%; dual CAR: 53:47%). Collectively, the dual CAR construct endowed T cells with cytotoxic efficiency against MM.1s^{BCMA+} tumors comparable with that of monotargeted BCMA CAR T cells.

Concern has been raised regarding induction of an allogeneic response against MM.1s tumor cells, which could obscure the antigen-specific reactivity of the CAR T cells.[18,49] However, during the

Figure 5. The dual CAR endows T cells with similar therapeutic efficacy as monotargeted BCMA CAR T cells against MM.1s *in vivo*

(A) Schematics of MM.1s^{BCMA+} xenotransplantation model treated with 2.5–3 × 10^6 CAR$^+$ T cells (i.v.) at day 7 after tumor inoculation. (B) Representative FACS plot of SP6, BCMA, and dual CAR T cells used in animal experiment. Percentage of CAR T cells is reported. Black contour plot, isotype; gray, SP6 CAR; blue, BCMA CAR; red, dual CAR. (C) Confirmation of an established tumor in NSG mice, visualized by bioluminescent imaging (BLI) at day 7 after MM.1s i.v. injection. Exposure time 300 s at day 7, followed by serial BLI exposures (120 s) in weekly intervals. (D) Average radiance ±SEM of BLI obtained from MM orthotopic regions of interest involving thoracic, pelvic, and hind leg bone regions. One representative experiment out of $n = 4$ independent experiments with $n = 4$ CAR T cell donors is given. SP6 CAR, $n = 13$; BCMA CAR, $n = 13$; dual CAR, $n = 15$ animals. Statistics calculated by Mann-Whitney test, outlier identified with ROUT (Q = 1%); n.s., not significant. (E) Tumor cell count (CD138$^+$GFP$^+$ cells), CD3$^+$ T cells, and CAR T cells in flushed BM. Significance calculated by Mann-Whitney test. $^*p < 0.05$, $^{**}p < 0.01$; n.s., not significant. (F) Geometric mean fluorescence intensity (gMFI) of PD-1, LAG-3, and TIM-3 exhaustion markers in CD3 cells in BM. In (E) and (F), mean values ± SEM, $n = 3$ independent experiments, data points represent individual animals.

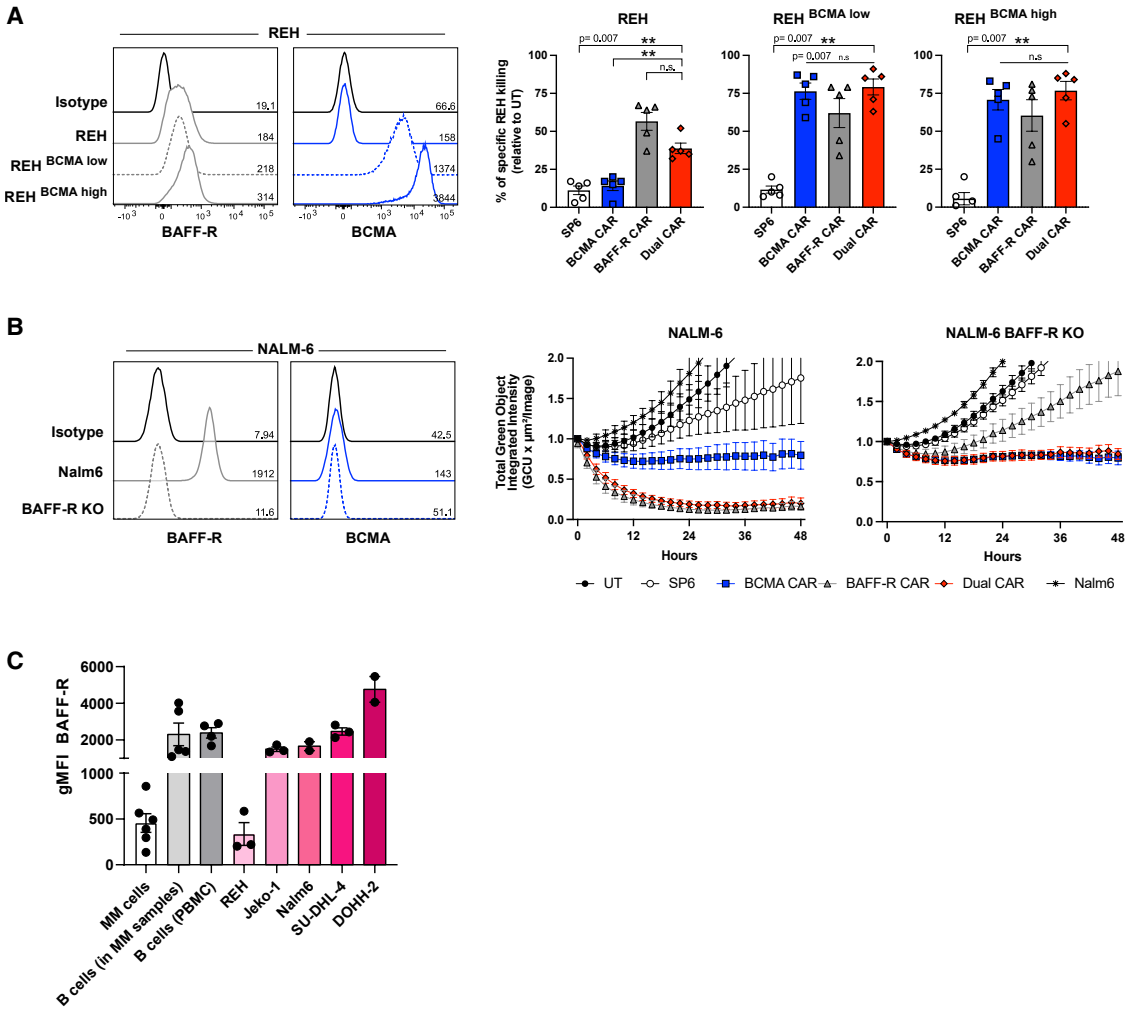

Figure 6. Dual CAR T cells can rescue cytolytic efficacy in BCMA-deficient cell lines expressing BAFF-R

(A) Left: BAFF-R (gray) and BCMA (blue) antigen expression on REH and engineered REH$^{BCMA\ low}$ and REH$^{BCMA\ high}$ tumor cells (isotype control, black open histogram). Mouse anti-human BCMA clone 19F2 antibody was used. gMFI values for the tested antigen are reported. Right: FACS-based cytotoxicity assay of CAR T cells and REH, REH$^{BCMA\ low}$, REH $^{BCMA\ high}$ in 1:1 coculture. Specific REH killing is reported as a percentage and it is calculated relative to coculture with UT. Data are mean ± SEM, significance calculated by Mann-Whitney test, data points represent single CAR T cell donors. *N* = 2–3 independent experiments performed. (B) BAFF-R (gray) and BCMA (blue) antigen expression on NALM-6 and NALM- 6$^{BAFF-R\ KO}$ tumor cells. Anti-BCMA clone 19F2 antibody was used. gMFI values for the tested antigen are reported. Right panel: IncuCyte assay of CAR T cells in coculture with GFP^{+} NALM-6 cells. UT, SP6 CAR, BCMA CAR, BAFF.R CAR, dual CAR, *n* = 5 CAR T cell donors; *n* = 7 independent experiments performed. For NALM-6 $^{BAFF-R\ KO}$ cells: UT, SP6 CAR, BCMA CAR, BAFF.R CAR, dual CAR, *n* = 3 CAR T cell donors; *n* = 5 independent experiments performed. Data are mean ± SEM. (C) Quantification of BAFF-R antigen density on various B cell lines, primary B cells, or MM cells. Flow cytometry data are given as gMFI, data points are independent primary cell donors, or for the cell lines, independent biological replicates.

observation period of 21 days, we obtained a clear advantage for the BCMA CAR and dual CAR T cells over the control SP6 CAR T cells, thus making an allogeneic effect against MM.1s cells unlikely.

Bispecific CAR T cells rescue anti-MM cytolytic activity when BCMA is lost but BAFF-R is expressed

To compare the activity of the anti-BAFF-R scFv in dual CAR T cells with the single BAFF-R CAR, REH cells (BAFF-R^{+}BCMA^{-}) were engineered to express low (REH$^{BCMA\ low}$) and high (REH$^{BCMA\ high}$) amounts of BCMA (Figure 6A). Specific killing of REH was induced by BAFF-R CAR and dual CAR T cells at similar efficacy, but not by BCMA CAR T cells. In the presence of both antigens, regardless of high or low BCMA expression, the dual CAR T cell killing capacity was comparable with both monotargeted CAR constructs (Figure 6A, right and middle panel). In agreement, NALM-6 cells (BCMA^{-} BAFF-R^{+}) with an engineered deletion of BAFF-R (NALM-6 BAFF-R KO) were spared from anti-BAFF-R CAR and dual CAR T cell destruction (Figure 6B). To assess the antigen sensitivity of the scFv-targeting BAFF-R, we quantified BAFF-R antigen densities by determining gMFI values in various B cell populations.

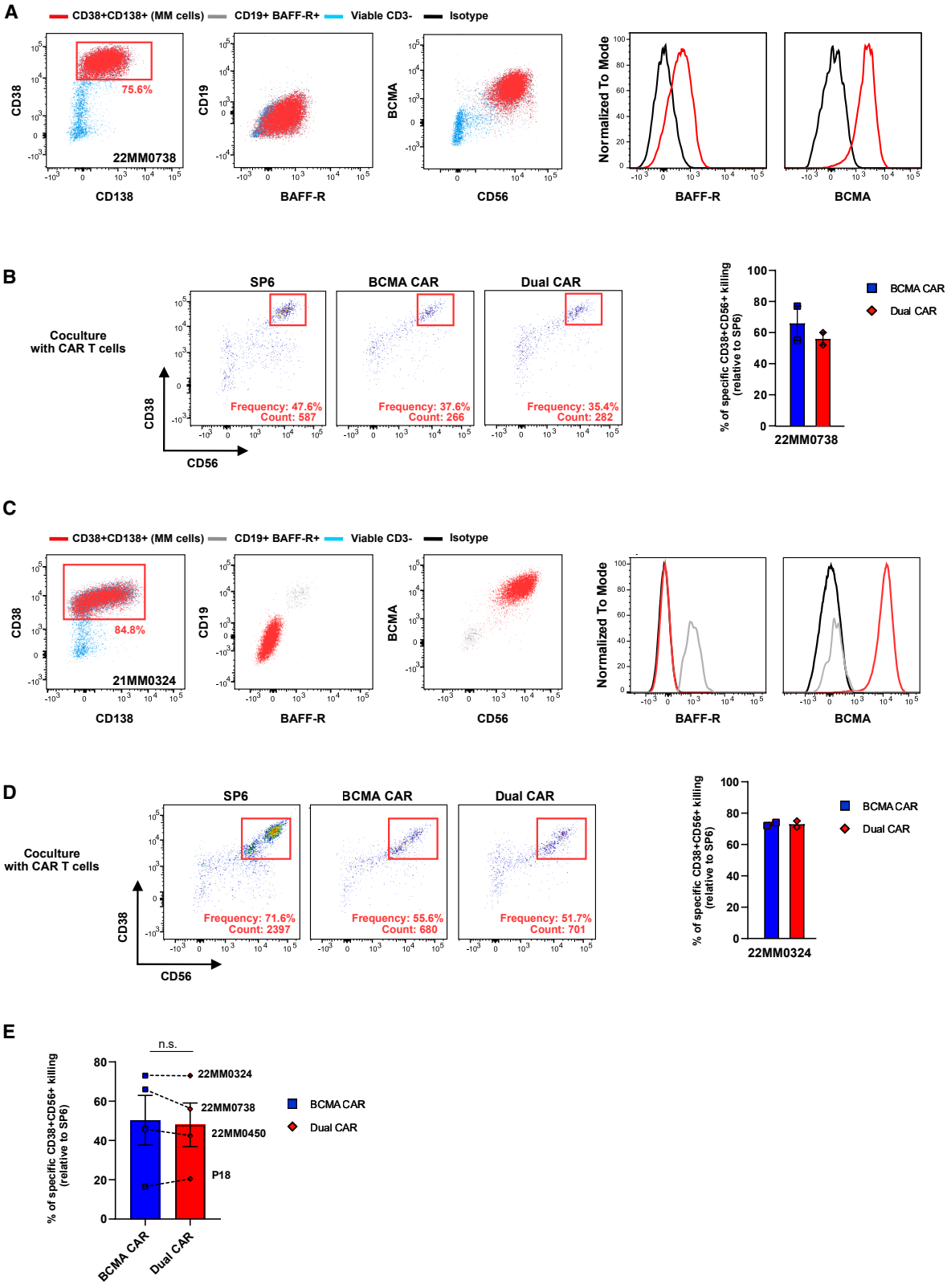

(legend on next page)

REH cells exhibited much lower values than B-NHL cell lines, primary B cells, or MM cells; however, they were efficiently lysed by BAFF-R CAR and dual CAR T cells, indicating their potency to be activated upon moderate antigen densities (Figures 6A and 6C).

Next, to further resolve antigen sensitivity NALM-6 cells were engineered to express BCMA and BAFF-R at various antigen density combinations (Figure S9A). Analysis of antigen-dependent killing confirmed that low amounts of BCMA and BAFF-R endowed monotargeted and dual CAR T cells with efficient cytolytic potency, which could only modestly be increased by higher amounts of BAFF-R or BCMA (Figures S9B–S9E). LAMP-1 degranulation revealed a reduced sensitivity of the monotargeted BAFF-R CAR T cells (LAMP-1$^+$: 20%–30%) compared with BCMA CAR T cells (LAMP-1$^+$: 50%–60%) when stimulated with low amounts of BAFF-R and BCMA, respectively (Figures S9D and S9E; right panel). Degranulation capacity of the BAFF-R CAR correlated with the BAFF-R antigen density on NALM-6 cells, visible as a stepwise increase in reactivity (Figure S9F, middle panel). In the dual CAR T cells, the percentage of degranulation was much less dependent on BAFF-R density, indicating the leading role of the BCMA scFv. We conclude that the anti-BCMA scFv has a dominant effect on dual CAR T cell avidity.

Dual CAR T cells efficiently deplete BAFF-R and BCMA double-positive primary patient MM cells

We examined the cytolytic efficacy of CAR T cells against primary MM cells obtained from BM. All specimens were first characterized by FACS for the presence of CD138$^+$CD38$^{+(high)}$ PCs, and PCs were further gated for BCMA and CD56 co-expression which covers the largest proportion of MM cells. This population was then analyzed for BAFF-R and BCMA expression (Figures 7A and 7C). Because of the highly variable frequencies of viable MM cells within the complex cell mixture of BM biopsies, killing rates were calculated relative to the SP6 control CAR T cells.[50] In addition, the endogenously high apoptosis rate of primary MM cells in overnight cultures allowed the evaluation of only half of the eight primary samples in flow cytometry-based killing assays. BCMA CAR and dual CAR T cells exhibited a substantially higher cytolytic efficacy against CD38$^{+(high)}$CD56$^+$ PCs than control SP6 CAR T cells (Figures 7B and 7D). Pairwise comparison indicated a similar potency of the BCMA CAR and dual CAR T cells (Figure 7E).

Dual CAR T cells can control tumor growth in an antigen escape model *in vivo*

BCMA loss or downregulation in MM cells can occur even before anti-BCMA CAR T cells impose immunoselection.[5,6,51,52] To mimic this immune escape scenario *in vivo*, we used the aforementioned MM.1s$^{\text{BCMA KO BAFF-R+}}$ cell line. We opted on employing a cell population with residual amounts of BCMA$^+$ cells alongside transgenic BAFF-R expression to compare the functionality of the BCMA CAR and the dual CAR. We hypothesized a superior efficacy of the dual CAR when challenged by tumor cells exhibiting both antigens at various densities, as observed *in vitro* (Figure 4K).

To establish the growth capacity of BCMA-silenced MM.1s cells, NSG mice received the MM.1s$^{\text{BCMA KO BAFF-R+}}$ tumor cell line (Figure 8A; cell line characterized in Figure 4D). After confirmed tumor cell engraftment, animals were treated with 3×10^6 CAR T cells (Figure 8B). On day 7 after CAR T cell injection, minimal or weak signal of malignant cells was detected in dual CAR T cell-treated mice, but BCMA CAR T cell recipients showed a higher tumor burden, pronounced in the pelvic region (Figures 8C and 8D). On day 21, the dual CAR-treated group exhibited much stronger tumor regression compared with the BCMA CAR group (average radiance value BCMA CAR: 2.9×10^7; dual CAR: 1.6×10^4; untransduced [UT]: 1.8×10^7). Animals were sacrificed on day 27; however, very low tumor burden prohibited the analysis of marker expression on residual MM.1s cells. Together, mixed MM.1s$^{\text{BCMA KO BAFF-R+}}$ tumor cells grew properly in NSG mice and could be challenged with antigen-specific CAR T cells. Extended observation periods for the growth of CRISPR-Cas9-engineered MM.1s cells may elicit allogeneic CAR T cell effects.[18,49]

Next, to rule out an allorejection against CRISPR-Cas9-modified MM.1s$^{\text{BCMA KO BAFF-R+}}$ tumor cells, that could obscure the specificity and efficiency of the dual CAR, an SP6 CAR control was included and the observation period was terminated at day 14 (Figure 8E). Notably, to prove the robustness of the antigen escape model, the composition of the mixed tumor cell population regarding the frequency of BCMA KO cells was different from the previous experiment (Figures 8A and 8F; see also Figure 4D). Furthermore, an independent T cell donor was used. Consistent with the previous experiment, BLI revealed a superior tumor growth control of the dual CAR at days 7 and 14, compared with the BCMA CAR and

Figure 7. Dual CAR T cells have high cytolytic activity against patient-derived MM cells *in vitro*

(A) Gating strategy for the detection and characterization of malignant PCs (CD138$^+$CD38$^+$ in red) within BM-derived MM sample (no. 22MM0738). Further gating on malignant PCs defined as BCMA$^+$ CD56$^+$ in red. The frequency of malignant PCs in BM specimens is reported for each donor. On the right, in the histogram the red line indicates BAFF-R and BCMA positivity among the gated PC population; black open histogram, isotype control. (B) Corresponding to the donor in (A), gating strategy of FACS-based killing assay of CAR T cells and primary BM of MM patients. CAR T cells were stained with intravital cell dye eFluor670. MM cells were detected by eFluor670$^-$ CD38^{high} CD56$^+$ expression. Frequency in percent and total cell numbers of remaining malignant PCs in coculture after 18 h is reported. On the right, bar graph for quantification of FACS-based cytotoxicity assay of CAR T cells and primary BM of MM patients in 1:1 E:T coculture. Specific malignant PC killing (eFluor670$^-$ CD38^{high} CD56$^+$) is reported as a percentage and it is calculated relative to coculture with SP6 CAR T cells. Data points represent single CAR T cell donors. (C and D) Exactly as in (A and B), gating strategy (C) and killing assay (D) were performed with an independent primary MM target cell population (no. 21MM0324). (E) Bar graph for quantification of FACS-based cytotoxicity assays; in total eight independent MM specimens were tested, four generated quantifiable data. Cytolytic efficacy was not significantly different between both CAR T cell groups, as calculated by Mann-Whitney test.

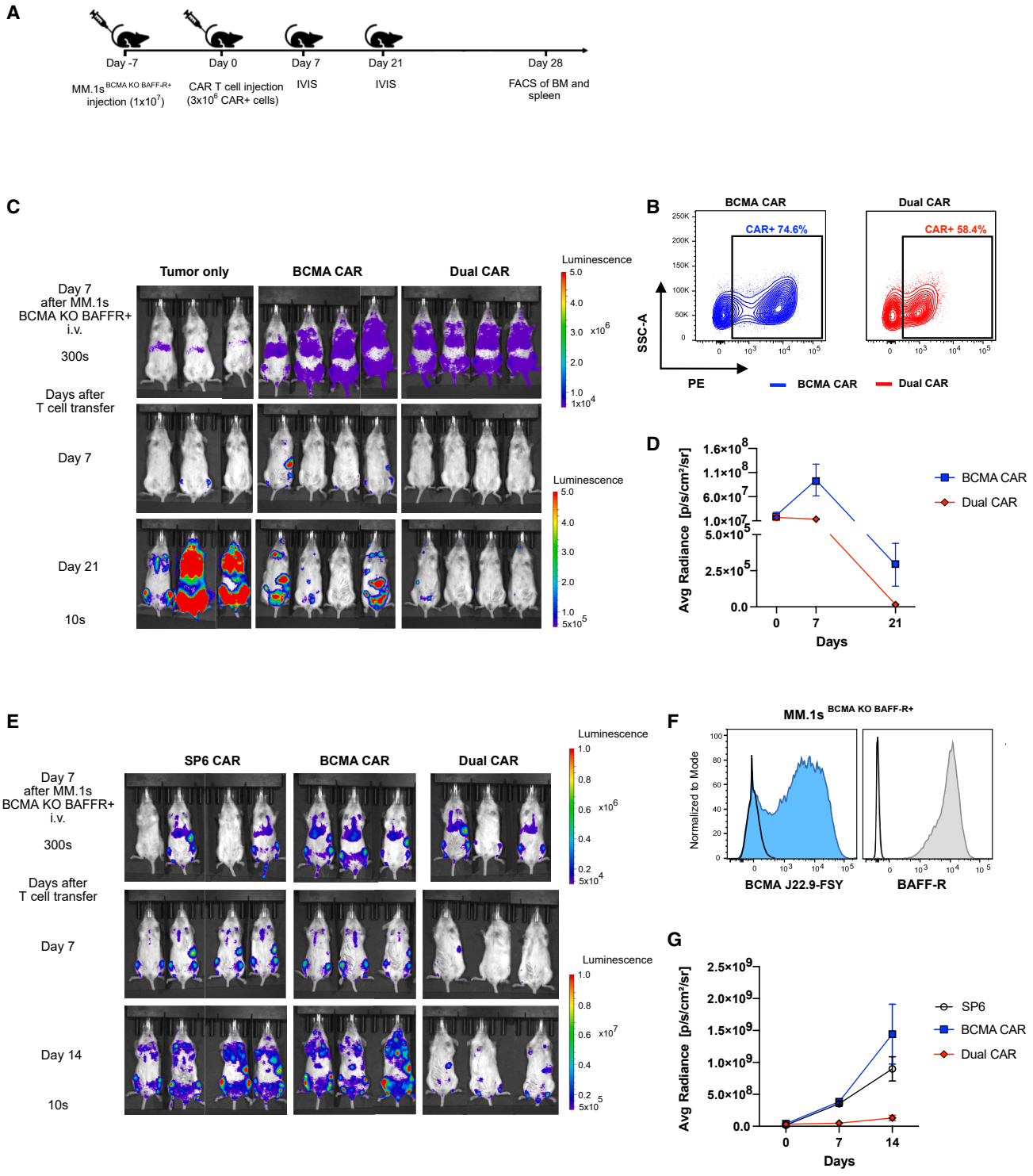

Figure 8. Bispecific CAR T cells can compensate for the loss of BCMA and sustain tumor growth control

(A) Schematics of a MM.1s$^{BCMA\ KO\ BAFF-R+}$ xenotransplantation model treated with 2.5–3 × 10^6 CAR$^+$ T cells (i.v.) on day 7 after tumor inoculation. (B) FACS plot of BCMA CAR and dual CAR T cells used in animal experiment (A). Percentage of CAR T cells is reported. Gates for CAR positivity are set relative to untransduced T cells; blue contour plot, BCMA CAR; red, dual CAR. T cell numbers for injection were normalized for CAR expression, all animals received the same numbers of CAR$^+$ T cells. CARs detected by anti-human IgG-PE staining. (C) Confirmation of an established tumor in NSG mice, visualized by BLI at day 6 after MM.1s$^{BCMA\ KO\ BAFF-R+}$ i.v. injection. Exposure time 300 s,

(legend continued on next page)

SP6 CAR control groups (Figure 8G; average radiance value BCMA CAR: 1.4×10^9; dual CAR: 1.3×10^8; SP6 CAR: 9×10^8). Collectively, dual CAR T cells directed against BCMA and BAFF-R control efficiently MM.1s growth under challenging conditions that are more likely to occur in patients bearing heterogeneous MM tumor cell populations.

DISCUSSION

In this study we demonstrate the identification of BAFF-R as a marker for the heterogeneous immunophenotypes of MM adding to the classification of MM cell subsets and, ultimately, to the outcome prediction of patients with aggressive disease. We validated the rationale and feasibility of simultaneously targeting BAFF-R and BCMA with a dual targeting CAR T cell platform. We suggest that the bispecific targeting has the potential to mitigate immune escape and to confer a deep remission state by co-targeting a distinct B cell-like phenotype among MM cells.

The role of the BAFF-R in malignant PC transformation has not been fully appreciated. Its restricted expression to mature B cells between the progenitor and the PC stages of development makes it a potential target for immunotherapies.[14,41,42,53–56] BAFF-R is essential for B cell growth and differentiation; hence, evasion of malignant B cells from anti-BAFF-R-targeted immunotherapies by downregulation seems less likely.[57] Accordingly, BAFF-R has been recently demonstrated as a promising target for the treatment of B cell neoplasms.[42] Evidence of BAFF-R expression in MM can be found in a seminal paper from Novak et al.[25] However, whole-exome sequencing, copy-number profiling, cytogenetics, and scRNA-seq studies have shown that MM is characterized by an inherent subclonal and temporal heterogeneity.[26,27,32,58,59]

In accordance with BAFF-R gene (*TNFRSF13C*) expression in a specific clonal or temporal PC,[60] our study demonstrated the expression of BAFF-R on MM cells at several levels from gene to protein. A re-examination of a large scRNA-seq database revealed *TNFRSF13C* expression in a sizable number of MM patients, with higher prevalence in cases with advanced and dismal prognosis.[26,27] Importantly, among malignant *TNFRSF13C*-expressing cells, about half did not co-express *TNFRSF17* (BCMA) confirming the existence of distinct subpopulations in MM. Analysis of DEG between *TNFRSF13C*$^+$ and *TNFRSF13C*$^-$ MM cells uncovered several driver gene functions that could contribute to increased resistance of *TNFRSF13C*-proficient cells. Pathways affected involved apoptosis resistance, cell growth, and immunomodulation. For instance, upregulation of HLA-E, which interacts with CD94/NKG2A, can dampen the activity of patrolling NK cells. Thus, BAFF-R$^+$ malignant PCs can potentially evade NK cell immunosurveillance and gain further immunoresistance.[35] Our longitudinal analysis of an MM patient cohort with LTS pointed to the predictive value of *TNFRSF13C* expression at first diagnosis. Lower gene expression correlated with a significantly higher probability for maintaining a durable CR. Thus, quantification of *TNFRSF13C* mRNA and BAFF-R protein in NDMM cases could aid in deciding whether a targeted immunotherapy against BAFF-R is warranted. Furthermore, we validated BAFF-R expression on CD138$^+$ malignant PCs by IHC. These data were corroborated by a surface marker panel that resolved heterogeneous MM immunophenotypes. UMAP representation of pooled FACS data on pregated CD38$^+$CD138$^+$ malignant PC confirmed that only half of them expressed BCMA in a BAFF-R$^+$BCMA$^-$ cluster.

Dual CAR T cell therapies are designed to provide cytotoxic functions even when one target antigen is lost or downregulated.[8,9,61] In line with this, BAFF-R targeting has been proposed to overcome CD19 loss in B-ALL.[42] Along tumor evolution, therapy-imposed pressure may select for less-differentiated PCs with a higher degree of molecular and cytogenetic alterations.[60,62–64] Therefore, when challenged with monotargeted BCMA CAR T cells, residual BCMA$^-$ MM cells can predispose to a shorter PFS. We envision that identification and targeting of BAFF-R as a complementary target at ID will enhance elimination of a heterogeneous tumor in an early treatment line.

In this scenario, we took advantage of a high avidity BCMA scFv,[21] and a BAFF-R scFv with proven preclinical and clinical efficacy[42] to generate dual CAR constructs with complementary properties. While BCMA targeting covers the largest population of clonotypic mature PCs, the BAFF-R scFv aims for the elimination of a less-prevalent MM tumor cell subset with potentially B cell-like features. For in-depth functional characterization, we opted for a bispecific CAR construct in a tandem configuration which combined high transduction rates, cytolytic activity triggered by both scFvs, and compensation for BCMA loss when BAFF-R was expressed. The reactivity of the dual CAR construct against BCMA$^+$ target cells was equivalent to the monotargeted BCMA CAR T cells, which can be explained by the high avidity of these effector cells. This result is in contrast to a tandem CD19/CD79a CAR showing compromised activity against each target antigen when only CD19 or CD79a were expressed.[65] MM.1s^{BCMA+} tumor growth *in vivo* was equally controlled by both the BCMA CAR and the dual CAR T cells, confirming that the functionality of BCMA scFv was preserved in the tandem CAR design. Using NALM-6 cells with titrated amounts of both target antigens, we revealed that for dual CAR T cells even at very low expression of BCMA affected degranulation capacity, which could not be enhanced by further increase in antigen expression. For the BAFF-R, maximal degranulation was stimulated only at high antigen

followed by serial BLI exposures (10 s) in intervals as indicated. (D) Average radiance ± SEM of BLI obtained from MM orthotopic regions of interest involving thoracic, pelvic, and hind leg regions. Data from all animals shown in (D). (E) Visualization of MM.1s$^{BCMA\ KO\ BAFF-R+}$ tumor growth. Injection of SP6 CAR, BCMA CAR, and dual CAR T cells at day 7 after tumor injection. In weekly intervals, BLI exposures until day 14 after CAR T cell injection. (F) BCMA and BAFF-R expression on MM.1s$^{BCMA\ KO\ BAFF-R+}$ cells used for the experiment in (E). The antibody J22.9-FSY was used for BCMA detection. (G) Average radiance ± SEM of BLI obtained from MM orthotopic regions of interest involving thoracic, pelvic, and hind leg regions.

densities. Interestingly, in a syngeneic mouse model, an anti-murine BAFF-R/BCMA dual CAR failed to eliminate an MM cell line when target antigens were only weakly expressed, a feature that could be compensated for by engineered secretion of IL-18.[66]

Clinical response data suggest that BCMA remains the prime target for CAR T and CAR NK cells in MM. In a recent study, scRNA-seq data were broadly cross-validated by whole-exome sequencing, bulk RNA sequencing, and a proteomics approach filtering for surface proteins.[32] Consistent with their clinical consideration for CAR T and CAR NK cell targeting, *TNFRSF17* (BCMA), *SDC1* (CD138), *FCRL5*, *CD38*, *SLAMF7* (CS1), and *CD79A* were the top-ranking genes upregulated in PCs. Other primary targets with lower average gene expression in PCs included CD19 and BAFF-R. Although the latter are expressed with lesser prevalence in PCs, it seems feasible that their concurrent overexpression in B cells may gain therapeutic benefit because a putative B cell development reservoir of malignant PCs could be simultaneously targeted.[32] In view of the multitude of MM-associated antigens, in a preclinical study it has been shown that iPSC-derived NK cells can accommodate quadruple CRISPR-Cas9-mediated gene editing that would allow for a CAR-mediated simultaneous targeting of an even greater number of MM surface antigens.[67]

The myeloma initiating cell (MIC) concept has harnessed some debate about the molecular and immunophenotypic features of such cells. MM cells that represent terminally differentiated PCs are identifiable by morphology and surface markers that are routinely employed in clinical diagnostics, but earlier B cell differentiation states such as post-GC pre-PC B cells may lack CD138 ($CD19^+CD20^+CD138^-CD38^-$) and have already clonotypic and oncogenic MIC potential. Likewise, other evidences have pointed to a $CD19^-CD20^-CD138^+CD38^+$ plasmablast population possessing tumor stem cell-like properties featuring plasticity regarding oncogenetic changes.[68] With CD19 CAR T cells eliciting responses in some cases of R/R MM, it was suggested that putative stem-like MM cells may express CD19.[13,69] In our scRNA-seq and FACS analysis, little evidence of $CD19^+$ malignant PCs was found, but the hypothesis that $BAFF\text{-}R^+$ MM cells may represent a MIC-like subpopulation still remains to be proven. We confirmed the efficacy of simultaneously targeting $BCMA^+BAFF\text{-}R^+$ cells in primary human MM samples. Despite differences in tumor load and intensity of BAFF-R and BCMA expression, the dual CAR T cells efficiently eliminated the MM population to the same extent as BCMA CAR T cells. In an antigen escape model, we used the $MM.1s^{BCMA\ KO\ BAFF\text{-}R+}$ cell line to mimic BCMA antigen loss. Staining with the high-affinity J22.9-FSY antibody, but not with the commonly used antibody clone 19F2, revealed that a proportion of $MM.1s^{BCMA\ KO\ BAFF\text{-}R+}$ retained BCMA expression. This heterogeneity makes the cell line suitable to phenocopy aspects of primary human MM samples. In an IncuCyte assay, the dual CAR exhibited the most pronounced killing, while the monotargeted BCMA CAR clearly lagged behind. Thus, simultaneous antigen stimulation defined the activation threshold for dual CAR T cells.

In vitro reactivity of the dual CAR translated into *in vivo* efficacy against the $MM.1s^{BCMA\ KO\ BAFF\text{-}R+}$ tumor. At day 7, BCMA CAR- and SP6 CAR T cell-treated mice showed substantially higher tumor load than the dual CAR-treated group. This difference was even more pronounced 14 days after CAR T cell injection. We conclude that dual CAR T cells prevent the selective growth advantage of BCMA-low or -negative tumor cells, provided that these cells express BAFF-R.

In conclusion, we envision that a synchronous targeting of BAFF-R and BCMA has strong complementary therapeutic effects. Since BCMA-negative MM tumor cells can preexist prior to immunotherapy, a dual targeting approach has the greatest benefit when applied in the same treatment line as conventional monotargeted BCMA CARs. In this state, a greater opportunity for preventing a selective advantage of BCMA escape mutants exists. The second indication is the R/R state, where BAFF-R-positive target cells have increased in frequency. We suggest that deeper eradication of MM cells featuring lack of BCMA and gain of BAFF-R may translate into deeper minimal residual disease, and, subsequently, a longer patient survival.

METHODS

Construction of bispecific CARs

The fully humanized anti-BCMA CAR was used identical as described.[21] Briefly, the VH and VL sequences are derived from the antibody J22.9-FSY scFv, they were connected via a Whitlow linker, the CAR backbone consists of a human IgG1 (amino acids 266–503) hinge region with mutated Fc-γ binding region, a CD28 transmembrane domain, and a CD3ζ activation domain. The anti-BAFF-R scFv was derived from the fully humanized anti-BAFF-R CAR,[42] and a synthesized gene sequence was cloned into the same CAR backbone using NotI and MfeI restriction sites. All constructs were assembled in the retroviral vector MP71.[21]

A bispecific "anti-BAFF-R/BCMA CAR-IgG1mut-28ζ" in tandem configuration was constructed by connecting the anti-BAFF-R scFv with the BCMA scFv using a $(Gly_4Ser)_4$ linker. The construct was codon-optimized (GeneArt, Thermo Fisher). Preceded by a CD3 leader peptide, the construct was synthesized and cloned into the same CAR backbone as the anti-BCMA CAR.

Bioinformatic analysis

Analysis of single-cell sequencing data. The two publicly available single-cell datasets used were downloaded from GEO (GSE117156 and GSE161195), filtered (nFeatureRNA > 200, nCountRNA < 10000, percent.mt < 50, percent.Ig > 3, COL1A2 == 0, TRAC = = 0,C1QA = = 0, S100A8 == 0, GATA1 == 0), normalized and integrated by experiment with Seurat 5 using RPCA. Where applicable in the preprocessing steps, 30 dimensions were used.

Differential gene expression was performed with Seurat using MAST and a cutoff min.pct = 0.001. Genes were considered differentially

expressed, when they exceeded an absolute log2 fold change of 0.2 and subseeded a multiple testing corrected p value of 1.0e−20. For differences between *TNFRSF13C*-positive and *TNFRSF13C*-negative cells by subgroup, we applied min.pct = 0.1, logfc.threshold = 0.25 and an adjusted p value of 0.05 as cutoff for differential expression.

Functional analysis was performed using gProfiler and fGSEA.[70,71] As input for gProfiler DEGs were separated into genes upregulated in *TNFRSF13C*-positive and upregulated in *TNFRSF13C*-negative cells.

For fGSEA we used sign(log2FC) * −log10(padj) * (2abs(log2FC)) for ranking.

FACS data

Integrated analysis of FACS data is based on pre-selected viable cells found positive for CD38 and CD138. Using the R package "CytoTree" (v.1.0.3) the data were transformed with arcsinh using a cofactor of 150 and an individually determined compensation transformation for each of the four markers used for UMAP construction.[72]

Mice

Male and female NSG mice (NOD.Cg-Prkcd^{scid}Il2rg$^{tm1\ Wjl}$/SzJ) mice were purchased from Jackson ImmunoResearch Laboratories, and further bred under pathogen-free conditions at the Max Delbrück Center. NXG mice (NOD-Prkcd^{scid}Il2rg^{tm1}/Rj) were purchased from Janvier Laboratories (France). Animals were used at an age between 8 and 12 weeks, and treatment cohorts were age and sex matched.

Retroviral vector production

Anti-BCMA, anti-BAFF-R, dual and bicistronic CARs as well as the BAFF-R encoding retroviral vectors were produced by transient transfection of HEK2937T cells followed by transduction of stable packaging cell line 293VecGalV. For transient retrovirus production, HEK293T cells were transfected using the $CaPO_4$ precipitation method with plasmids encoding for gag and pol (pcDNA 3.1), env gene 10A1 (pALF-10A1GaV), and the respective CAR encoding MP71 plasmid. After 48 h, retroviral supernatant (SN) was collected, filtered (0.45 μm), and used for transduction of 293VecGalV cells to generate stable retrovirus producing packaging cell lines. Stable producer cells were sorted for high CAR expression by goat anti-human IgG-PE (Southern Biotech) staining by FACS, expanded, and frozen. Aliquots of the collected viral supernatants were filtered, frozen, and stored at −80°C. Producer cells were maintained in DMEM containing 10% FCS, 1% pen/strep, and 1% Na-Pyr.

Human T cell transduction

Human peripheral blood mononuclear cells (PBMCs) were purified using Pancoll solution (PAN-Biotech). PBMCs were cultured in T cell medium (TCM) containing RPMI-1640, 10% FCS (PAN-Biotech), 1 mM NaPyr, 0.1 mM non-essential amino acids, 100 U/mL penicillin, 100 μg/mL streptomycin (all Thermo Fisher Scientific). UT control cells were prepared in parallel and subjected to the same protocol except that TCM instead of viral SN was used for transduction. Depending on whether the human T cells were used *in vivo* or *in vitro* experiments, they were cultured either with IL-7/IL-15 (10 ng/mL each), or IL-2 (100 IU/mL), respectively (all Miltenyi Biotec). PBMCs were activated for 2 days with 10 μL of TransAct reagent/1 × 10^6 cells (Miltenyi Biotec). For transduction, RetroNectin (TaKaRa)-coated plates were prepared. On the day of the first transduction, viral SN was added and the plates were centrifuged (2,000 × g, 2 h, 32°C). Afterward, activated T cells were transferred to the virus-coated plates, mixed with viral SN (1:1) supplemented with either IL-7/IL-15 or IL-2 and the plates were centrifuged (800 × g, 20 min, 32°C). Next day, a second transduction round was performed. On day 10, T cells were cultured at a density of 2 × 10^6/mL in fresh TCM with low IL-2 (10 U/mL). On day 14, T cells were frozen and stored in liquid nitrogen. Cell cultures supplemented with IL-7/IL-15 were terminated at day 10, and then frozen prior to *in vitro* and *in vivo* assays. CAR expression was detected using polyclonal PE-labeled goat anti-human IgG. *In vitro*, CAR T cell expansion and cell yield for CAR constructs directed against BAFF-R, BCMA, or dual CARs were similar.

Primary MM patient samples and BM from healthy donors

Forty primary samples were derived from BM aspirates of MM patients (n = 35), and benign BM from femoral head (n = 5) of patients undergoing hip arthroplasty. BM aspirates from MM patients were taken either from newly diagnosed cases or R/R cases. For flow cytometry analysis, evaluation did not make a distinction.

Mononuclear cells of BM aspirates and collagenase-treated and scratched BM from femoral heads were purified using Pancoll solution (PAN-Biotech). Leukocytes were collected and FcR blocking was performed for 20 min at RT with TruStain FcX in FACS buffer (PBS, 2% FCS, 10 mM EDTA). Antibodies (all BioLegend) were added and samples were incubated for 30 min at RT. After incubation, cells were washed with FACS buffer and analyzed. Dead cells were excluded by staining with 7-AAD (Thermo Fisher Scientific). Data were acquired with the Miltenyi MACSQuant 10 flow cytometer and analyzed with FlowJo 10 software. The staining panel for the detection of PC and B cells is given in Tables S2 and S3.

IHC

Tissue samples from 58 patients with MM were retrieved from the files of the Institute of Pathology, University of Würzburg, Germany. We analyzed representative formalin-fixed, decalcified, and paraffin-embedded BM biopsies. Biopsies from extramedullary MM manifestations did not require decalcification. All cases had been analyzed for establishing the diagnosis with a panel of immunostains including CD138, Igκ, lgλ, CD20, CD3, CD56, and cyclin D1. To evaluate BAFF-R expression on neoplastic PCs, we compared the CD138 and BAFF-R immunostains to assess the percentage of labeled PCs. As BAFF-R is normally expressed on B cells, we also compared BAFF-R expression patterns with CD20 immunostains. PCs could be easily recognized due to their characteristic

cytomorphological features. In addition, CD20 expression was usually more intense in B cells than in BAFF-R-expressing neoplastic PCs. For this study anti-BAFF-R rabbit recombinant monoclonal antibody (Abcam, Cambridge, UK, clone no. EPR 14633) in a dilution 1:200 was used. All immunostains were performed in a Leica-Bond III automated immunostainer using manufacturer-supplied reagents and protocols. The following cohort of MM patients (collection of PC myeloma patients) was analyzed.

- 20 cases with biopsies performed at time of diagnosis (NDMM).
- 20 cases with biopsies performed during the disease course in pretreated patients.
- 10 cases with more than 2 follow-up biopsies performed during the course of the disease.
- 8 cases in the final disease stage presenting with extramedullary manifestations.

Human cell lines

The human MM cell lines OPM-2 (ACC50), RPMI-8226 (ACC402), and NCI-H923 (ACC163) together with B-NHL cell lines Jeko-1 (ACC533) and DOHH-2 (ACC47) were purchased from DSMZ (Braunschweig, Germany). MM cell line MM.1s (CRL-2974) was purchased from ATCC. The B cell precursor leukemia cell lines NALM-6 (ACC128) and REH (ACC22) were kindly provided by Dr. Stephan Mathas (MDC, Berlin, Germany); their identity was confirmed by a multiplex cell line authentication test (Multiplexion, Heidelberg, Germany). Jurkat NF-KB-eGFP reporter cells were kindly provided by Dr. Sophie Marinoff (Glycotope, Berlin, Germany). All cell lines were cultured in RPMI-1640 medium, supplemented with 10% FCS, 2 mM L-glutamine, sodium pyruvate, and penicillin/streptomycin. MM.1s, NALM-6, Jeko-1, and DOHH-2 were engineered to express eGFP and luciferase as previously described.[21] All cell lines were expanded upon receipt and aliquots were frozen in liquid nitrogen. Mycoplasma testing by PCR was done periodically. Cell lines were tested for BCMA and BAFF-R expression with BCMA (CD269-clone 19F2) and BAFF-R (CD268-clone11C1) antibodies.

REH BCMA$^{low/high}$ were generated with the sleeping beauty (SB) transposon technology using the Amaxa Cell line Nucleofector Kit V and following the manufacturer's instructions. Briefly, REH were electroporated with an SB-MP71-hBCMA plasmid containing the SB recognition sites and an SB transposase vector. BCMA^{+} cells were sorted in order to distinguish low and high BCMA expression. Similarly, also NALM-6 BCMA^{+} cell lines were generated with SB technology. Afterward, NALM-6 BAFF-R$^{low\text{-}mid\text{-}high}$ BCMA$^{low\text{-}mid\text{-}high}$ were isolated by progressive cell sorting, applying fixed sorting gates on low-mid-high BCMA/BAFF-R intensity.

BAFF-R knockout (KO) in NALM-6 and BCMA KO in MM.1s cells were obtained by CRISPR-Cas9-mediated editing. Briefly, the gRNA complex was prepared by mixing the crRNA (HS.Cas9TNFRS17.1.AB or BAFF-R) and the trans-activating CRISPR-RNA (tracRNA) to reach 100 μM final concentration. gRNA was annealed in a thermocycler at 95°C for 5 min, aliquots were made and stored at −20°C. The ribonucleoprotein complex was assembled mixing the gRNA and the Cas9 protein in a ratio 2:1 and poly(L-glutamic acid) was added as enhancer. NALM-6 or MM.1S cells (5×10^6) were resuspended in this mixture. The MAXCyte ATx electroporation system was used for transfection following the manufacturer's instructions.

MM.1S$^{BCMA\ BAFF\text{-}R+}$ and MM.1S$^{BCMA\ KO\ BAFF\text{-}R+}$ transgenic cell lines were generated by retroviral transduction with viral supernatants collected form VecGalV MP71 BAFF-R stable producer cell lines as mentioned before. Transduced cells were sorted for BAFF-R positivity and expanded. Aliquots were frozen in liquid nitrogen. Sequences for CRISPR-Cas9 editing are given:

target: *TNFRSF17*; crRNA sequence: GCGATTCTCTGGACCTGTTT (IDT design)

target: *TNFRSF13C*; crRNA sequence: CTCACCGTCCTTGTCTCCGT (custom-made; IDT)

Flow cytometry-based cytotoxicity assay

In vitro cytotoxicity of CAR T cells against tumor cell lines was analyzed by flow cytometry. Briefly, T cells were cocultured with tumor cell lines in a 1:1 ratio (2.5×10^4 cells per well each) in a 96-well U-bottom plate in TCM medium. All samples were performed in duplicates. After 18 h, duplicates were pooled and washed with PBS. Dead cells were detected using 7-AAD and tumor cells were detected by GFP. Data were acquired with the Miltenyi MACSQuant 10 flow cytometer and analyzed with FlowJo 10 software. Specific target tumor cell line killing was calculated as percentage relative to coculture with UT T cells as follows:

$$\%\ \text{specific target cell line killing} = 1 - (\text{target cell count in coculture with CAR Tcells} \div \text{target cell line count in coculture with UT}).$$

In vitro cytotoxicity of CAR T cells against primary MM samples composed of heterogeneous cell subpopulations was analyzed differently. Prior to coculture, CAR T cells were labeled with intravital cell dye eFluor670 (1:20,000; Thermo Fisher, eBioscience) following the manufacturer's instructions. eFluor670^{+} CAR T cells were

cocultured with primary MM samples in a 1:1 ratio (2.5×10^4 cells per well each) in a 96-well U-bottom plate. All samples were performed in duplicates. After 18 h, duplicates were pooled and washed with PBS. Dead cells were detected using 7-AAD. Cells were stained and data were acquired with the Miltenyi MACSQuant 10 flow cytometer and analyzed with FlowJo 10 software. Residual viable MM cells were identified as eFluor^{670-}CD38^{high}CD56^{+}. Specific MM cell killing was calculated as percentage relative to coculture with negative control SP6 CAR as following:

% of specific MM cell killing = 1 − (target cell count in coculture with CAR T cells ÷ target cell count in coculture with SP6).

For the detection and discrimination of CAR T and target cells, the antibody panel in combination with fluorescent cell dyes is given in Table S3.

Real-time quantification of *in vitro* cytotoxicity

A 96-well flat-bottom plate was coated with 0.01% poly-L-lysine for 1 h at 37° C. After washing the plate with PBS, GFP-expressing target cells (2.5×10^4 cells per well each) and T cells at an E:T ratio of 1:1 were seeded. Cells were allowed to settle for 2 h at 37°C before starting imaging in an IncuCyte system (Sartorius) every 2 h over a total time frame of 48 h. Total green object integrated intensity (GCU × μm^2/image) was quantified and normalized to the first data point. Loss of GFP signal intensity was interpreted as killing of the GFP$^+$ target cells. All samples were performed in duplicates. Tumor cells without addition of CAR T cells were used as controls.

Degranulation assay

T cells were cocultured with target cells in a 96-well U-bottom plate in a 1:1 ratio (2.5×10^4 cells per well each) for 2 h at 37°C. Anti-human LAMP-1 (CD107a) antibody (cl. H4A3, BD Biosciences), brefeldin A (10 mg/mL, Sigma-Aldrich), and monensin/Golgi-Stop (0.7 μg/mL, BD Biosciences), was added directly to the coculture. At the end of the stimulation period, cells were washed once in PBS and stained with anti-human CD4 (cl. OKT4, BioLegend) and CD8 (cl. SK1, BioLegend) antibodies. To distinguish the target cells, either GFP-expressing target cells or staining with an anti-human CD38 (cl. HIT2, BioLegend) antibody was used. Antigen-independent maximal release was achieved by incubation of CAR T cells with ionomycin (1 μM) and phorbol-12-myristate-13-acetate (PMA 5 ng/mL). Minimum release represents CAR T cells incubated without target cells in TCM. Calculation of specific T cell degranulation was achieved according to the formula:

% of T cell degranulation = (experimental degranulation – spontaneous degranulation) × 100
÷ (maximum degranulation – spontaneous degranulation).

Cytokine secretion assay

Antigen-stimulated cytokine secretion by human CAR T cells was performed as described.[21] Briefly, CAR T cells were cocultured with tumor cell lines in a 1:1 ratio (2.5×10^4 cells per well each) in 96-well plates for 18 h. All samples were performed in duplicates. The concentration of human IFN-γ in coculture supernatants was determined by enzyme-linked immunosorbent assays according to the manufacturer's instructions (BD Bioscience). Antigen-independent maximal release was achieved by incubation of T cells with ionomycin (1 μM) and PMA (5 ng/mL). Minimum release represents T cells incubated without target cells.

MM xenotransplantation model

MM.1S^{BCMA+} or MM.1S$^{BCMA\ KO\ BAFF\text{-}R+}$ (0.8×10^7 to 1×10^7 cells) were injected i.v. into NSG mice (NOD.Cg-PrkdcscidIl2rgtm1 Wji/SzJ, Jackson ImmunoResearch Laboratories or Janvier). All cell lines contained GFP and luciferase activity. Tumor growth was monitored using luciferin (Biosynth) i.p. application and *in vivo* BLI (IVIS spectrum imaging system; Caliper Life Sciences), essentially as described.[21,73] On day 7, tumor engraftment was confirmed by BLI and afterward CAR T cells $2.5–3 \times 10^7$ were administered i.v. Tumor progression was monitored on the days indicated in the figure legends. Mice were imaged for several exposure times, ranging between 1 and 300 s. Binning and exposure were adjusted to achieve maximum sensitivity without leading to image saturation. To analyze the bioluminescence signal flux for each mouse as average radiance (p/s/cm2/sr), the Living Image software version 4.5 (Caliper Life Sciences) was used. BLI represented tumor manifestations in the BM and thorax, and thus signal intensity was measured in regions of interest that encompassed the MM orthotopic thoracic and pelvic regions of each individual mouse. Animals were sacrificed on the days indicated in the figure legends. Tumor cells and remaining human CAR T cells were detected and analyzed in the BM and spleen. To analyze BM cells, femora were dissected and flushed with PBS while spleens were meshed. The cell suspension was applied to a 70-μm cell strainer, centrifuged and lysed with hypotonic ammonium-chloride-potassium erythrocyte lysis buffer. Subsequently, cells were analyzed by flow cytometry. Cells isolated from BM and spleen were counted with the Miltenyi MACSQuant 10 flow cytometer and analyzed with BD FACS Symphony A3. The antibody panel used for analysis of T cells and MM.1s tumor cells is given in Table S4.

Statistical analysis

All of the statistical details of experiments can be found in the figures, figure legends, results, and supplemental figures, including the statistical tests used, and the exact value of n (representing number of animals per sample and number of experimental replicates). Results are expressed as arithmetic means ± SEM if not otherwise stated. Values of $p < 0.05$ were considered statistically significant, as determined by the unpaired Mann-Whitney U test; $^{*}p < 0.05$, $^{**}p < 0.01$, $^{***}p < 0.001$. Analyses were performed using Prism (GraphPad Software, v.6.0, 9.0), R (v.3.6.1), or Bioconductor 3.9.

DATA AND CODE AVAILABILITY

- The scRNA-seq datasets are publicly available as referenced.
- The remaining data are available within the article and supplemental information.
- Materials generated in this study are available from the corresponding author upon reasonable request.
- A Material Transfer Agreement might be required, solely for use of materials in preclinical applications.
- For additional questions, please contact arehm@mdc-berlin.de.

ACKNOWLEDGMENTS

We are grateful to K. Gerlach and M. Schrimpf for help in cell culture, and A. Wirges, H.-P. Rahn, and K. Rautenberg for expert technical assistance in flow cytometry. A.R. and U.E.H. received research funds from Fate Therapeutics, San Diego, CA. H.E. was supported by an MD student stipend from Berliner Krebsgesellschaft, Berlin, Germany. J.P.O.-A. received funding for a fellowship from the EU's Horizon 2020 Research and Innovation Programme under the Marie Sklodowska-Curie grant agreement number 101034290 (EMERALD International PhD Program for Medical Doctors). An Institutional Review Board at Charite-University Medicine Berlin and from Berliner Ärztekammer approved the acquisition from human healthy donor PBMCs, buffy coats, leukapheresis material, diagnosed MM patient's BM samples, benign BM samples from hip arthroplasty. Sex and race were not used as a variable in study analyses, and study findings are not specific to one sex or race. The recruitment process did not involve a selection bias. Specimen for IHC were obtained from the archives of the Institute of Pathology, University of Würzburg, Germany. The study was conducted according to the Declaration of Helsinki and in accordance with local ethical guidelines; written informed consent of all patients was obtained. All the samples were de-identified. An approval for recruiting voluntary, healthy blood donors has been obtained from Ethikausschuss 1 am Campus Charité–Mitte (EA1/003/17; EA1/222/13) and Ethikausschuss am Campus Virchow-Klinikum (EA2/216/18). Approval for bone marrow biopsies was obtained from Ärztekammer Berlin, Eth-13/23. All animal studies were performed according to institutional and Berlin State guidelines of the "Landesamt für Gesundheit und Soziales" (LAGeSo) Berlin (G0279/19; G0331/19).

AUTHOR CONTRIBUTIONS

A.R. and U.E.H. conceived the study. A.F., K.Z., U.E.H., and A.R. wrote the manuscript. A.F., K.Z., A.L., I.A., L.M., J.P.O.-A., H.E., J.J., F.G., S.H., U.E.H., and A.R. performed the experiments. K.Z. and L.M. analyzed publicly available datasets. J.K., J.W., I.A., A.R., J.F., and U.-J.T. identified the clinical patients. A.F. and J.W. developed the flow panels used for patient myeloma phenotyping. M.B. designed the dual CAR constructs. L.K., X.W., Z.D., and S.C. developed and provided the BAFF-R CAR. All authors including A.R., J.R., E.P., and B.V. contributed intellectually to the experiments as well as editing and approval of the final version of the manuscript.

DECLARATION OF INTERESTS

A.R. and U.E.H. filed a patent application for the BCMA CAR used in this manuscript (WO2017211900-A1), they have equity ownership in CARTemis Therapeutics GmbH. L.K. filed a patent application for the BAFF-R CAR (WO2017214167-A1), he has equity ownership in Pepromene Bio., Inc. A.R. and U.E.H. received research funds from Fate Therapeutics, San Diego, CA. J.R., E.P., and B.V. are employees of Fate Therapeutics. The funding organizations had no influence on the study design, conduct of study, data generation, or data interpretation.

SUPPLEMENTAL INFORMATION

Supplemental information can be found online at https://doi.org/10.1016/j.ymthe.2025.12.005.

REFERENCES

1. Parikh, R.H., and Lonial, S. (2023). Chimeric antigen receptor T-cell therapy in multiple myeloma: A comprehensive review of current data and implications for clinical practice. CA Cancer J. Clin. *73*, 275–285. https://doi.org/10.3322/caac.21771.

2. Rasche, L., Wäsch, R., Munder, M., Goldschmidt, H., and Raab, M.S. (2021). Novel immunotherapies in multiple myeloma - chances and challenges. haematol. *106*, 2555–2565. https://doi.org/10.3324/haematol.2020.266858.

3. Minnie, S.A., and Hill, G.R. (2020). Immunotherapy of multiple myeloma. J. Clin. Invest. *130*, 1565–1575. https://doi.org/10.1172/JCI129205.

4. Raje, N., Berdeja, J., Lin, Y., Siegel, D., Jagannath, S., Madduri, D., Liedtke, M., Rosenblatt, J., Maus, M.V., Turka, A., et al. (2019). Anti-BCMA CAR T-Cell Therapy bb2121 in Relapsed or Refractory Multiple Myeloma. N. Engl. J. Med. *380*, 1726–1737. https://doi.org/10.1056/NEJMoa1817226.

5. Berdeja, J.G., Madduri, D., Usmani, S.Z., Jakubowiak, A., Agha, M., Cohen, A.D., Stewart, A.K., Hari, P., Htut, M., Lesokhin, A., et al. (2021). Ciltacabtagene autoleucel, a B-cell maturation antigen-directed chimeric antigen receptor T-cell therapy in patients with relapsed or refractory multiple myeloma (CARTITUDE-1): a phase 1b/2 open-label study. Lancet *398*, 314–324. https://doi.org/10.1016/S0140-6736(21)00933-8.

6. Munshi, N.C., Anderson, L.D., Jr., Shah, N., Madduri, D., Berdeja, J., Lonial, S., Raje, N., Lin, Y., Siegel, D., Oriol, A., et al. (2021). Idecabtagene Vicleucel in Relapsed and Refractory Multiple Myeloma. N. Engl. J. Med. *384*, 705–716. https://doi.org/10.1056/NEJMoa2024850.

7. Martin, T., Usmani, S.Z., Berdeja, J.G., Agha, M., Cohen, A.D., Hari, P., Avigan, D., Deol, A., Htut, M., Lesokhin, A., et al. (2023). Ciltacabtagene Autoleucel, an Anti-B-cell Maturation Antigen Chimeric Antigen Receptor T-Cell Therapy, for Relapsed/Refractory Multiple Myeloma: CARTITUDE-1 2-Year Follow-Up. J. Clin. Oncol. *41*, 1265–1274. https://doi.org/10.1200/JCO.22.00842.

8. Samur, M.K., Fulciniti, M., Aktas Samur, A., Bazarbachi, A.H., Tai, Y.T., Prabhala, R., Alonso, A., Sperling, A.S., Campbell, T., Petrocca, F., et al. (2021). Biallelic loss of BCMA as a resistance mechanism to CAR T cell therapy in a patient with multiple myeloma. Nat. Commun. *12*, 868. https://doi.org/10.1038/s41467-021-21177-5.

9. Da Via, M.C., Dietrich, O., Truger, M., Arampatzi, P., Duell, J., Heidemeier, A., Zhou, X., Danhof, S., Kraus, S., Chatterjee, M., et al. (2021). Homozygous BCMA gene deletion in response to anti-BCMA CAR T cells in a patient with multiple myeloma. Nat. Med. *27*, 616–619. https://doi.org/10.1038/s41591-021-01245-5.

10. Wang, D., Wang, J., Hu, G., Wang, W., Xiao, Y., Cai, H., Jiang, L., Meng, L., Yang, Y., Zhou, X., et al. (2021). A phase 1 study of a novel fully human BCMA-targeting CAR (CT103A) in patients with relapsed/refractory multiple myeloma. Blood *137*, 2890–2901. https://doi.org/10.1182/blood.2020008936.

11. Mailankody, S., Devlin, S.M., Landa, J., Nath, K., Diamonte, C., Carstens, E.J., Russo, D., Auclair, R., Fitzgerald, L., Cadzin, B., et al. (2022). GPRC5D-Targeted CAR T Cells for Myeloma. N. Engl. J. Med. *387*, 1196–1206. https://doi.org/10.1056/NEJMoa2209900.

12. Fernandez de Larrea, C., Staehr, M., Lopez, A.V., Ng, K.Y., Chen, Y., Godfrey, W.D., Purdon, T.J., Ponomarev, V., Wendel, H.G., Brentjens, R.J., et al. (2020). Defining an Optimal Dual-Targeted CAR T-cell Therapy Approach Simultaneously Targeting BCMA and GPRC5D to Prevent BCMA Escape-Driven Relapse in Multiple Myeloma. Blood Cancer Discov. *1*, 146–154. https://doi.org/10.1158/2643-3230.BCD-20-0020.

13. Garfall, A.L., Cohen, A.D., Susanibar-Adaniya, S.P., Hwang, W.T., Vogl, D.T., Waxman, A.J., Lacey, S.F., Gonzalez, V.E., Fraietta, J.A., Gupta, M., et al. (2023). Anti-BCMA/CD19 CAR T Cells with Early Immunomodulatory Maintenance for Multiple Myeloma Responding to Initial or Later-Line Therapy. Blood Cancer Discov. *4*, 118–133. https://doi.org/10.1158/2643-3230.BCD-22-0074.

14. Coquery, C.M., and Erickson, L.D. (2012). Regulatory roles of the tumor necrosis factor receptor BCMA. Crit. Rev. Immunol. *32*, 287–305. https://doi.org/10.1615/critrevimmunol.v32.i4.10.

15. Bossen, C., and Schneider, P. (2006). BAFF, APRIL and their receptors: structure, function and signaling. Semin. Immunol. *18*, 263–275. https://doi.org/10.1016/j.smim.2006.04.006.

16. Dhodapkar, K.M., Cohen, A.D., Kaushal, A., Garfall, A.L., Manalo, R.J., Carr, A.R., McCachren, S.S., Stadtmauer, E.A., Lacey, S.F., Melenhorst, J.J., et al. (2022). Changes in Bone Marrow Tumor and Immune Cells Correlate with Durability of Remissions Following BCMA CAR T Therapy in Myeloma. Blood Cancer Discov. *3*, 490–501. https://doi.org/10.1158/2643-3230.BCD-22-0018.

17. Ullah, M.A., and Mackay, F. (2023). The BAFF-APRIL System in Cancer. Cancers (Basel) *15*, 1791. https://doi.org/10.3390/cancers15061791.

18. Camviel, N., Wolf, B., Croce, G., Gfeller, D., Zoete, V., and Arber, C. (2022). Both APRIL and antibody-fragment-based CAR T cells for myeloma induce BCMA downmodulation by trogocytosis and internalization. J. Immunother. Cancer *10*, e005091. https://doi.org/10.1136/jitc-2022-005091.

19. Lee, L., Draper, B., Chaplin, N., Philip, B., Chin, M., Galas-Filipowicz, D., Onuoha, S., Thomas, S., Baldan, V., Bughda, R., et al. (2018). An APRIL-based chimeric antigen receptor for dual targeting of BCMA and TACI in multiple myeloma. Blood *131*, 746–758. https://doi.org/10.1182/blood-2017-05-781351.

20. Wong, D.P., Roy, N.K., Zhang, K., Anukanth, A., Asthana, A., Shirkey-Son, N.J., Dunmire, S., Jones, B.J., Lahr, W.S., Webber, B.R., et al. (2022). A BAFF ligand-based CAR-T cell targeting three receptors and multiple B cell cancers. Nat. Commun. *13*, 217. https://doi.org/10.1038/s41467-021-27853-w.

21. Bluhm, J., Kieback, E., Marino, S.F., Oden, F., Westermann, J., Chmielewski, M., Abken, H., Uckert, W., Höpken, U.E., and Rehm, A. (2018). CAR T Cells with Enhanced Sensitivity to B Cell Maturation Antigen for the Targeting of B Cell Non-Hodgkin's Lymphoma and Multiple Myeloma. Mol. Ther. *26*, 1906–1920. https://doi.org/10.1016/j.ymthe.2018.06.012.

22. Larson, R.C., Kann, M.C., Graham, C., Mount, C.W., Castano, A.P., Lee, W.H., Bouffard, A.A., Takei, H.N., Almazan, A.J., Scarfó, I., et al. (2023). Anti-TACI single and dual-targeting CAR T cells overcome BCMA antigen loss in multiple myeloma. Nat. Commun. *14*, 7509. https://doi.org/10.1038/s41467-023-43416-7.

23. Hildebrand, J.M., Luo, Z., Manske, M.K., Price-Troska, T., Ziesmer, S.C., Lin, W., Hostager, B.S., Slager, S.L., Witzig, T.E., Ansell, S.M., et al. (2010). A BAFF-R mutation associated with non-Hodgkin lymphoma alters TRAF recruitment and reveals new insights into BAFF-R signaling. J. Exp. Med. *207*, 2569–2579. https://doi.org/10.1084/jem.20100857.

24. Thompson, J.S., Bixler, S.A., Qian, F., Vora, K., Scott, M.L., Cachero, T.G., Hession, C., Schneider, P., Sizing, I.D., Mullen, C., et al. (2001). BAFF-R, a newly identified TNF receptor that specifically interacts with BAFF. Science *293*, 2108–2111. https://doi.org/10.1126/science.1061965.

25. Novak, A.J., Darce, J.R., Arendt, B.K., Harder, B., Henderson, K., Kindsvogel, W., Gross, J.A., Greipp, P.R., and Jelinek, D.F. (2004). Expression of BCMA, TACI, and BAFF-R in multiple myeloma: a mechanism for growth and survival. Blood *103*, 689–694. https://doi.org/10.1182/blood-2003-06-2043.

26. Cohen, Y.C., Zada, M., Wang, S.Y., Bornstein, C., David, E., Moshe, A., Li, B., Shlomi-Loubaton, S., Gatt, M.E., Gur, C., et al. (2021). Identification of resistance pathways and therapeutic targets in relapsed multiple myeloma patients through single-cell sequencing. Nat. Med. *27*, 491–503. https://doi.org/10.1038/s41591-021-01232-w.

27. Ledergor, G., Weiner, A., Zada, M., Wang, S.Y., Cohen, Y.C., Gatt, M.E., Snir, N., Magen, H., Koren-Michowitz, M., Herzog-Tzarfati, K., et al. (2018). Single cell dissection of plasma cell heterogeneity in symptomatic and asymptomatic myeloma. Nat. Med. *24*, 1867–1876. https://doi.org/10.1038/s41591-018-0269-2.

28. Gross Even-Zohar, N., Pick, M., Hofstetter, L., Shaulov, A., Nachmias, B., Lebel, E., and Gatt, M.E. (2022). CD24 Is a Prognostic Marker for Multiple Myeloma Progression and Survival. J. Clin. Med. *11*, 2913. https://doi.org/10.3390/jcm11102913.

29. Robillard, N., Avet-Loiseau, H., Garand, R., Moreau, P., Pineau, D., Rapp, M.J., Harousseau, J.L., and Bataille, R. (2003). CD20 is associated with a small mature plasma cell morphology and t(11;14) in multiple myeloma. Blood *102*, 1070–1071. https://doi.org/10.1182/blood-2002-11-3333.

30. Zhan, F., Barlogie, B., Arzoumanian, V., Huang, Y., Williams, D.R., Hollmig, K., Pineda-Roman, M., Tricot, G., van Rhee, F., Zangari, M., et al. (2007). Gene-expression signature of benign monoclonal gammopathy evident in multiple myeloma is linked to good prognosis. Blood *109*, 1692–1700. https://doi.org/10.1182/blood-2006-07-037077.

31. Starlets, D., Gore, Y., Binsky, I., Haran, M., Harpaz, N., Shvidel, L., Becker-Herman, S., Berrebi, A., and Shachar, I. (2006). Cell-surface CD74 initiates a signaling cascade leading to cell proliferation and survival. Blood *107*, 4807–4816. https://doi.org/10.1182/blood-2005-11-4334.

32. Yao, L., Wang, J.T., Jayasinghe, R.G., O'Neal, J., Tsai, C.F., Rettig, M.P., Song, Y., Liu, R., Zhao, Y., Ibrahim, O.M., et al. (2023). Single-Cell Discovery and Multiomic Characterization of Therapeutic Targets in Multiple Myeloma. Cancer Res. *83*, 1214–1233. https://doi.org/10.1158/0008-5472.CAN-22-1769.

33. Hose, D., Rème, T., Meissner, T., Moreaux, J., Seckinger, A., Lewis, J., Benes, V., Benner, A., Hundemer, M., Hielscher, T., et al. (2009). Inhibition of aurora kinases for tailored risk-adapted treatment of multiple myeloma. Blood *113*, 4331–4340. https://doi.org/10.1182/blood-2008-09-178350.

34. Lu, M., Ge, Q., Wang, G., Luo, Y., Wang, X., Jiang, W., Liu, X., Wu, C.L., Xiao, Y., and Wang, X. (2018). CIRBP is a novel oncogene in human bladder cancer inducing expression of HIF-1alpha. Cell Death Dis. *9*, 1046. https://doi.org/10.1038/s41419-018-1109-5.

35. Liu, X., Song, J., Zhang, H., Liu, X., Zuo, F., Zhao, Y., Zhao, Y., Yin, X., Guo, X., Wu, X., et al. (2023). Immune checkpoint HLA-E:CD94-NKG2A mediates evasion of circulating tumor cells from NK cell surveillance. Cancer Cell *41*, 272–287.e9. https://doi.org/10.1016/j.ccell.2023.01.001.

36. Tarte, K., Zhan, F., De Vos, J., Klein, B., and Shaughnessy, J., Jr. (2003). Gene expression profiling of plasma cells and plasmablasts: toward a better understanding of the late stages of B-cell differentiation. Blood *102*, 592–600. https://doi.org/10.1182/blood-2002-10-3161.

37. Cottini, F., Rodriguez, J., Hughes, T., Sharma, N., Guo, L., Lozanski, G., Liu, B., Cocucci, E., Yang, Y., and Benson, D. (2022). Redefining CD56 as a Biomarker and Therapeutic Target in Multiple Myeloma. Mol. Cancer Res. *20*, 1083–1095. https://doi.org/10.1158/1541-7786.MCR-21-0828.

38. van Andel, H., Kocemba, K.A., Spaargaren, M., and Pals, S.T. (2019). Aberrant Wnt signaling in multiple myeloma: molecular mechanisms and targeting options. Leukemia *33*, 1063–1075. https://doi.org/10.1038/s41375-019-0404-1.

39. Sprynski, A.C., Hose, D., Caillot, L., Réme, T., Shaughnessy, J.D., Jr., Barlogie, B., Seckinger, A., Moreaux, J., Hundemer, M., Jourdan, M., et al. (2009). The role of IGF-1 as a major growth factor for myeloma cell lines and the prognostic relevance of the expression of its receptor. Blood *113*, 4614–4626. https://doi.org/10.1182/blood-2008-07-170464.

40. Lutz, R., Grünschläger, F., Simon, M., Awwad, M.H.S., Bauer, M., Yousefian, S., Beumer, N., Jopp-Saile, L., Sedlmeier, A., Solé-Boldo, L., et al. (2024). Multiple myeloma long-term survivors exhibit sustained immune alterations decades after first-line therapy. Nat. Commun. *15*, 10396. https://doi.org/10.1038/s41467-024-54543-0.

41. Rodig, S.J., Shahsafaei, A., Li, B., Mackay, C.R., and Dorfman, D.M. (2005). BAFF-R, the major B cell-activating factor receptor, is expressed on most mature B cells and B-cell lymphoproliferative disorders. Hum. Pathol. *36*, 1113–1119. https://doi.org/10.1016/j.humpath.2005.08.005.

42. Qin, H., Dong, Z., Wang, X., Cheng, W.A., Wen, F., Xue, W., Sun, H., Walter, M., Wei, G., Smith, D.L., et al. (2019). CAR T cells targeting BAFF-R can overcome CD19 antigen loss in B cell malignancies. Sci. Transl. Med. *11*, eaaw9414. https://doi.org/10.1126/scitranslmed.aaw9414.

43. Ferguson, I.D., Patiño-Escobar, B., Tuomivaara, S.T., Lin, Y.H.T., Nix, M.A., Leung, K.K., Kasap, C., Ramos, E., Nieves Vasquez, W., Talbot, A., et al. (2022). The surfaceome of multiple myeloma cells suggests potential immunotherapeutic strategies and protein markers of drug resistance. Nat. Commun. *13*, 4121. https://doi.org/10.1038/s41467-022-31810-6.

44. Marino, S.F., and Daumke, O. (2024). Structure-based humanization of a therapeutic antibody for multiple myeloma. J. Mol. Med. *102*, 1151–1161. https://doi.org/10.1007/s00109-024-02470-4.

45. Dong, Z., Budde, L.E., Oh, E., Szymura, S., Anderson, A., Del Real, M., Cha, S.C., Forman, S.J., Kwak, L.W., and Wang, X. (2024). Analysis of polyfunctionality for

enhanced BAFF-R CAR T-cell therapy for hematologic malignancies. Blood Adv. *8*, 4066–4076. https://doi.org/10.1182/bloodadvances.2024013195.

46. Lam, N., Finney, R., Yang, S., Choi, S., Wu, X., Cutmore, L., Andrade, J., Huang, L., Amatya, C., Cam, M., and Kochenderfer, J.N. (2023). Development of a bicistronic anti-CD19/CD20 CAR construct including abrogation of unexpected nucleic acid sequence deletions. Mol. Ther. Oncolytics *30*, 132–149. https://doi.org/10.1016/j.omto.2023.07.001.

47. Shukla, D., Gabunia, K., McGettigan, S.E., Patel, P.R., Christensen, S., Fan, T.J., Song, D., Luo, Y., Wang, Y., Wang, H., et al. (2025). CAR Binders Affect CAR T-cell Tonic Signaling, Durability, and Sensitivity to Target. Cancer Immunol. Res. *13*, 867–880. https://doi.org/10.1158/2326-6066.CIR-24-1347.

48. Frigault, M.J., Lee, J., Basil, M.C., Carpenito, C., Motohashi, S., Scholler, J., Kawalekar, O.U., Guedan, S., McGettigan, S.E., Posey, A.D., Jr., et al. (2015). Identification of chimeric antigen receptors that mediate constitutive or inducible proliferation of T cells. Cancer Immunol. Res. *3*, 356–367. https://doi.org/10.1158/2326-6066.CIR-14-0186.

49. Schmidts, A., Ormhøj, M., Choi, B.D., Taylor, A.O., Bouffard, A.A., Scarfò, I., Larson, R.C., Frigault, M.J., Gallagher, K., Castano, A.P., et al. (2019). Rational design of a trimeric APRIL-based CAR-binding domain enables efficient targeting of multiple myeloma. Blood Adv. *3*, 3248–3260. https://doi.org/10.1182/bloodadvances.2019000703.

50. Moles, M.W., Erdlei, H., Menzel, L., Massaro, M., Fiori, A., Bunse, M., Schrimpf, M., Gerlach, K., Gudipati, V., Reiser, J., et al. (2024). CXCR4 has a dual role in improving the efficacy of BCMA-redirected CAR-NK cells in multiple myeloma. Front. Immunol. *15*, 1383136. https://doi.org/10.3389/fimmu.2024.1383136.

51. Salem, D.A., Maric, I., Yuan, C.M., Liewehr, D.J., Venzon, D.J., Kochenderfer, J., and Stetler-Stevenson, M. (2018). Quantification of B-cell maturation antigen, a target for novel chimeric antigen receptor T-cell therapy in Myeloma. Leuk. Res. *71*, 106–111. https://doi.org/10.1016/j.leukres.2018.07.015.

52. Smith, E.L., Harrington, K., Staehr, M., Masakayan, R., Jones, J., Long, T.J., Ng, K.Y., Ghoddusi, M., Purdon, T.J., Wang, X., et al. (2019). GPRC5D is a target for the immunotherapy of multiple myeloma with rationally designed CAR T cells. Sci. Transl. Med. *11*, eaau7746. https://doi.org/10.1126/scitranslmed.aau7746.

53. Meyer-Bahlburg, A., Andrews, S.F., Yu, K.O.A., Porcelli, S.A., and Rawlings, D.J. (2008). Characterization of a late transitional B cell population highly sensitive to BAFF-mediated homeostatic proliferation. J. Exp. Med. *205*, 155–168. https://doi.org/10.1084/jem.20071088.

54. Mackay, F., Schneider, P., Rennert, P., and Browning, J. (2003). BAFF AND APRIL: a tutorial on B cell survival. Annu. Rev. Immunol. *21*, 231–264. https://doi.org/10.1146/annurev.immunol.21.120601.141152.

55. Ng, L.G., Sutherland, A.P.R., Newton, R., Qian, F., Cachero, T.G., Scott, M.L., Thompson, J.S., Wheway, J., Chtanova, T., Groom, J., et al. (2004). B cell-activating factor belonging to the TNF family (BAFF)-R is the principal BAFF receptor facilitating BAFF costimulation of circulating T and B cells. J. Immunol. *173*, 807–817. https://doi.org/10.4049/jimmunol.173.2.807.

56. Rickert, R.C., Jellusova, J., and Miletic, A.V. (2011). Signaling by the tumor necrosis factor receptor superfamily in B-cell biology and disease. Immunol. Rev. *244*, 115–133. https://doi.org/10.1111/j.1600-065X.2011.01067.x.

57. Schweighoffer, E., and Tybulewicz, V.L. (2018). Signalling for B cell survival. Curr. Opin. Cell Biol. *51*, 8–14. https://doi.org/10.1016/j.ceb.2017.10.002.

58. Bolli, N., Avet-Loiseau, H., Wedge, D.C., Van Loo, P., Alexandrov, L.B., Martincorena, I., Dawson, K.J., Iorio, F., Nik-Zainal, S., Bignell, G.R., et al. (2014). Heterogeneity of genomic evolution and mutational profiles in multiple myeloma. Nat. Commun. *5*, 2997. https://doi.org/10.1038/ncomms3997.

59. Lohr, J.G., Stojanov, P., Carter, S.L., Cruz-Gordillo, P., Lawrence, M.S., Auclair, D., Sougnez, C., Knoechel, B., Gould, J., Saksena, G., et al. (2014). Widespread genetic heterogeneity in multiple myeloma: implications for targeted therapy. Cancer Cell *25*, 91–101. https://doi.org/10.1016/j.ccr.2013.12.015.

60. Liu, R., Gao, Q., Foltz, S.M., Fowles, J.S., Yao, L., Wang, J.T., Cao, S., Sun, H., Wendl, M.C., Sethuraman, S., et al. (2021). Co-evolution of tumor and immune cells during progression of multiple myeloma. Nat. Commun. *12*, 2559. https://doi.org/10.1038/s41467-021-22804-x.

61. Ruella, M., and Maus, M.V. (2016). Catch me if you can: Leukemia Escape after CD19-Directed T Cell Immunotherapies. Comput. Struct. Biotechnol. J. *14*, 357–362. https://doi.org/10.1016/j.csbj.2016.09.003.

62. Fakhri, B., and Vij, R. (2016). Clonal Evolution in Multiple Myeloma. Clin. Lymphoma Myeloma Leuk. *16*, S130–S134. https://doi.org/10.1016/j.clml.2016.02.025.

63. Keats, J.J., Chesi, M., Egan, J.B., Garbitt, V.M., Palmer, S.E., Braggio, E., Van Wier, S., Blackburn, P.R., Baker, A.S., Dispenzieri, A., et al. (2012). Clonal competition with alternating dominance in multiple myeloma. Blood *120*, 1067–1076. https://doi.org/10.1182/blood-2012-01-405985.

64. Egan, J.B., Shi, C.X., Tembe, W., Christoforides, A., Kurdoglu, A., Sinari, S., Middha, S., Asmann, Y., Schmidt, J., Braggio, E., et al. (2012). Whole-genome sequencing of multiple myeloma from diagnosis to plasma cell leukemia reveals genomic initiating events, evolution, and clonal tides. Blood *120*, 1060–1066. https://doi.org/10.1182/blood-2012-01-405977.

65. Leung, I., Templeton, M.L., Lo, Y., Rajan, A., Stull, S.M., Garrison, S.M., Salter, A.I., Smythe, K.S., Correnti, C.E., Srivastava, S., et al. (2023). Compromised antigen binding and signaling interfere with bispecific CD19 and CD79a chimeric antigen receptor function. Blood Adv. *7*, 2718–2730. https://doi.org/10.1182/bloodadvances.2022008559.

66. Ng, B.D., Rajagopalan, A., Kousa, A.I., Fischman, J.S., Chen, S., Massa, A., Elias, H.K., Manuele, D., Galiano, M., Lemarquis, A.L., et al. (2024). IL-18-secreting multi-antigen targeting CAR T cells eliminate antigen-low myeloma in an immunocompetent mouse model. Blood *144*, 171–186. https://doi.org/10.1182/blood.2023022293.

67. Cichocki, F., Bjordahl, R., Goodridge, J.P., Mahmood, S., Gaidarova, S., Abujarour, R., Davis, Z.B., Merino, A., Tuininga, K., Wang, H., et al. (2022). Quadruple gene-engineered natural killer cells enable multi-antigen targeting for durable antitumor activity against multiple myeloma. Nat. Commun. *13*, 7341. https://doi.org/10.1038/s41467-022-35127-2.

68. Johnsen, H.E., Bogsted, M., Schmitz, A., Bodker, J.S., El-Galaly, T.C., Johansen, P., Valent, P., Zojer, N., Van Valckenborgh, E., Vanderkerken, K., et al. (2016). The myeloma stem cell concept, revisited: from phenomenology to operational terms. Haematologica *101*, 1451–1459. https://doi.org/10.3324/haematol.2015.138826.

69. Garfall, A.L., Maus, M.V., Hwang, W.T., Lacey, S.F., Mahnke, Y.D., Melenhorst, J.J., Zheng, Z., Vogl, D.T., Cohen, A.D., Weiss, B.M., et al. (2015). Chimeric Antigen Receptor T Cells against CD19 for Multiple Myeloma. N. Engl. J. Med. *373*, 1040–1047. https://doi.org/10.1056/NEJMoa1504542.

70. Kolberg, L., Raudvere, U., Kuzmin, I., Adler, P., Vilo, J., and Peterson, H. (2023). g:Profiler-interoperable web service for functional enrichment analysis and gene identifier mapping (2023 update). Nucleic Acids Res. *51*, W207–W212. https://doi.org/10.1093/nar/gkad347.

71. Subramanian, A., Tamayo, P., Mootha, V.K., Mukherjee, S., Ebert, B.L., Gillette, M.A., Paulovich, A., Pomeroy, S.L., Golub, T.R., Lander, E.S., and Mesirov, J.P. (2005). Gene set enrichment analysis: a knowledge-based approach for interpreting genome-wide expression profiles. Proc. Natl. Acad. Sci. USA *102*, 15545–15550. https://doi.org/10.1073/pnas.0506580102.

72. Dai, Y., Xu, A., Li, J., Wu, L., Yu, S., Chen, J., Zhao, W., Sun, X.J., and Huang, J. (2021). CytoTree: an R/Bioconductor package for analysis and visualization of flow and mass cytometry data. BMC Bioinformatics *22*, 138. https://doi.org/10.1186/s12859-021-04054-2.

73. Wirges, A., Bunse, M., Joedicke, J.J., Blanc, E., Gudipati, V., Moles, M.W., Shiku, H., Beule, D., Huppa, J.B., Höpken, U.E., and Rehm, A. (2022). EBAG9 silencing exerts an immune checkpoint function without aggravating adverse effects. Mol. Ther. *30*, 3358–3378. https://doi.org/10.1016/j.ymthe.2022.07.009.